Article

Current Biology

NF1 Is a Direct G Protein Effector Essential for Opioid Signaling to Ras in the Striatum

Highlights

- NF1 is a direct G protein effector inhibited by the Gβγ subunits
- Activation of the Ras-Akt-mTOR axis by opioid receptors in the striatum requires NF1
- Opioid receptors activate Ras only in direct pathway striatal neurons
- NF1 in striatal neurons regulates morphine reward

Authors

Keqiang Xie, Lesley A. Colgan, Maria T. Dao, ..., Roy G. Smith, Ryohei Yasuda, Kirill A. Martemyanov

Correspondence

kirill@scripps.edu

In Brief

Xie et al. describe a novel signaling mechanism that links opioid receptors to Ras signaling in the brain. They show that a key role in this process belongs to direct interaction of G protein βγ subunits with the key Ras regulator NF1. Acting in striatal neurons, NF1 determines the sensitivity of mice to rewarding effects of morphine administration.

Xie et al., 2016, Current Biology *26*, 2992–3003
November 21, 2016
http://dx.doi.org/10.1016/j.cub.2016.09.010

CellPress

CellPress

Current Biology
Article

NF1 Is a Direct G Protein Effector Essential for Opioid Signaling to Ras in the Striatum

Keqiang Xie,[1] Lesley A. Colgan,[2] Maria T. Dao,[3] Brian S. Muntean,[1] Laurie P. Sutton,[1] Cesare Orlandi,[1] Sanford L. Boye,[4] Shannon E. Boye,[4] Chien-Cheng Shih,[1] Yuqing Li,[5] Baoji Xu,[1] Roy G. Smith,[3] Ryohei Yasuda,[2] and Kirill A. Martemyanov[1,6,*]

[1]Department of Neuroscience, The Scripps Research Institute, 130 Scripps Way, Jupiter, FL 33458, USA
[2]Max Planck Florida Institute for Neuroscience, 1 Max Planck Way, Jupiter, FL 33458, USA
[3]Department of Metabolism and Aging, The Scripps Research Institute, 120 Scripps Way, Jupiter, FL 33458, USA
[4]Department of Ophthalmology, University of Florida, 1395 Center Drive, Gainesville, FL 32610, USA
[5]Department of Neurology, University of Florida, 1600 SW Archer Road, Gainesville, FL 32610, USA
[6]Lead Contact
*Correspondence: kirill@scripps.edu
http://dx.doi.org/10.1016/j.cub.2016.09.010

SUMMARY

It is well recognized that G-protein-coupled receptors (GPCRs) can activate Ras-regulated kinase pathways to produce lasting changes in neuronal function. Mechanisms by which GPCRs transduce these signals and their relevance to brain disorders are not well understood. Here, we identify a major Ras regulator, neurofibromin 1 (NF1), as a direct effector of GPCR signaling via Gβγ subunits in the striatum. We find that binding of Gβγ to NF1 inhibits its ability to inactivate Ras. Deletion of NF1 in striatal neurons prevents the opioid-receptor-induced activation of Ras and eliminates its coupling to Akt-mTOR-signaling pathway. By acting in the striatal medium spiny neurons of the direct pathway, NF1 regulates opioid-induced changes in Ras activity, thereby sensitizing mice to psychomotor and rewarding effects of morphine. These results delineate a novel mechanism of GPCR signaling to Ras pathways and establish a critical role of NF1 in opioid addiction.

INTRODUCTION

Neural circuits rely on the neurotransmitter-signaling systems for processing information flow that ultimately drives behavioral reactions. As a central input nucleus of the basal ganglia system, the striatum is crucially involved in initiating and maintaining movement, formation of habits, valuation of reward, and mediating the effects of addictive drugs [1, 2]. The striatum receives diverse and abundant neurotransmitter inputs from multiple brain regions, which converge on medium spiny projection neurons (MSN), a major cell type in the region. Many of these inputs mediate their effects by activating G-protein-coupled receptors (GPCRs) abundantly expressed by MSNs [3]. GPCRs transduce their signals via a conserved mechanism dissociating heterotrimeric G proteins into Gα and Gβγ subunits, which in turn regulate downstream "effector" molecules [4]. It is thought that neurotransmitter-bound GPCRs activate distinct effectors that lead to unique physiological adaptations in MSNs and impose on behavior by producing lasting changes in the properties of striatal circuits [2]. However, the molecular and cellular mechanisms by which striatal GPCRs induce these changes are not well understood.

Several striatal GPCRs are capable of activating kinase pathways typically involved in cellular differentiation, growth, proliferation, and survival (e.g., Akt, mTOR, and mitogen-activated protein kinase [MAPK]), and this signaling is known to play a crucial role in regulating multiple aspects of striatal physiology, including excitability, synaptic plasticity, and spine architecture [5, 6]. Several "transactivation" mechanisms have been proposed to link GPCR activation with modulation of kinase pathways and have illustrated important roles for Gβγ and Ras in this process [7–9]. The activity of Ras is controlled by guanine nucleotide exchange factors (GEFs), which stimulate the exchange of guanosine diphosphate (GDP) for guanosine triphosphate (GTP), and by GTPase-activating proteins (GAPs), which terminate the active state by stimulating GTP hydrolysis [10]. In the active GTP-bound state, Ras binds effectors (e.g., Raf and phosphatidylinositol 3-kinase [PI3K]) to activate downstream signaling cascades (i.e., MAPK-ERK1/2 and Akt-mTOR). Both GEFs and GAPs are multidomain proteins and are subject to regulation by extracellular signals to allow for changes in Ras activity in response to changes in the environment [10]. Neurotransmitter-controlled regulation of Ras activity is essential for neuronal physiology, and its disruption underlies many neuropsychiatric conditions [5, 6].

Striatal function is substantially modulated by the opioid system [11, 12]. Striatal neurons express endogenous opioid peptides, endorphins, enkephalins, and dynorphin, which exert their effects by acting on GPCRs μ-, δ-, and κ- opioid receptors (MORs, DORs, and KORs), respectively [13]. As the target for exogenous opiate morphine, MOR plays a central role in controlling reward behavior, nociception, and development of dependence [11, 12]. Activation of MOR is known to indirectly affect striatal physiology by disinhibiting dopamine neurons in the ventral tegmental area that send their projections to the ventral striatum, thereby increasing dopaminergic tone [11, 12]. Notably, MORs are also prominently expressed in MSNs [14,

15], and recent evidence indicates that direct action of MOR in the striatum plays a pivotal role in opioid-mediated reward behavior [16]. Activation of MOR by morphine and/or endogenous opioid peptides markedly affects neuronal physiology, inducing changes in synaptic plasticity, dendritic spine morphology, and intrinsic excitability [17, 18]. Many of these long-term changes in physiology require signaling to Ras and its downstream kinase pathways [19]. Indeed, morphine markedly regulates multiple kinase pathways downstream from Ras, and this coupling is thought to contribute to the lasting nature of changes induced by exposure to opioids [20, 21]. However, the molecular mechanisms of Ras activation by opioid receptors in the striatal neurons and behavioral implications of this process remain obscure.

In this study, we identified a novel mechanism for the Ras activation by GPCRs, operating in the striatal neurons. Specifically, we found that Gβγ subunits when released upon activation of MOR bind and inhibit the activity of key Ras GAP protein neurofibromin (NF1), thereby leading to Ras activation. Elimination of NF1 completely prevented the ability of morphine to activate Ras and downstream Akt-mTOR/GSK3β-signaling pathway in the striatum. Furthermore, mice with disruption of striatal NF1 showed blunted responses to rewarding, but not analgesic, properties of morphine. These results reveal a critical role for NF1 in coupling neuronal GPCR signaling to Ras and suggest important implications of this process in the striatum for understanding drug addiction.

RESULTS

NF1 Is a Novel G Protein Effector Regulated by μ-Opioid Receptor Signaling

We hypothesized that the regulation of Ras by opioid receptors in the striatum may involve modulation of proteins, which directly control Ras activity. Among several known GEFs and GAPs regulating Ras activity, we found NF1 to be prominently expressed in the striatum. Fluorescence in situ hybridizations revealed high levels of NF1 to be present in most striatal neurons. Furthermore, all neurons containing MOR also co-expressed NF1 (Figures S1A and S1B).

To begin probing potential involvement of NF1 in opioid signaling, we first examined whether NF1 is sensitive to changes in the activity of MOR. HEK293 cells expressing Venus-based plasma membrane reporter construct were transfected with MOR and luciferase-tagged NF1, and changes in bioluminescence resonance energy transfer (BRET) were used to monitor changes in the proximity of NF1 to the plasma membrane (Figure 1A). The stimulation of cells with morphine resulted in a rapid increase in BRET signal ($1/\tau = 0.23 \pm 0.05\ s^{-1}$), suggesting NF1 recruitment to the plasma membrane (Figure 1B). Interestingly, a blockade of G protein βγ subunits with inhibitory peptide derived from GRK3 completely prevented NF1 translocation, suggesting that it is mediated by Gβγ (Figures 1B and 1C). Analysis of NF1 amino acid sequence revealed the presence of a bipartite module composed of a Sec14 homologous segment and a pleckstrin homology (PH)-like domain immediately adjacent to the RasGAP domain (Figure 1D). Because both PH and Sec14 domains have been shown to interact with Gβγ [22, 23], we next investigated the ability of NF1 to form complexes with Gβγ. First, we found that Gβγ and endogenous, full-length NF1 co-immunoprecipitated following Gβγ overexpression in HEK293T cells (Figure 1E). Second, the Sec14/PH module was sufficient for interaction with Gβγ in transfected cells (Figure 1F). Third, co-expression of Sec14/PH and Gβγ increased each other's levels, suggesting that binding between these two proteins is mutually stabilizing (Figure 1G). Finally, we demonstrated that a glutathione S-transferase (GST)-tagged recombinant Sec14/PH protein immobilized on beads could pull down purified recombinant Gβγ, indicating that the binding between the Sec14/PH module and Gβγ is direct (Figure 1H). We further confirmed specificity of Gβγ-NF1 interaction by showing that a dominant-negative construct (NF1-DN) comprising the minimal binding site (Sec14/PH) for Gβγ binding prevented association between Gβγ and full-length endogenous NF1 (Figure S1C).

In order to probe for Gβγ-Sec14/PH interaction in living cells, we measured BRET between Sec14/PH module and Gβγ (Figure 1I). Titration experiments revealed a hyperbolic increase in BRET signal that rapidly saturated with an increase in the acceptor/donor ratio (Figures 1I and 1J). In contrast, no significant increase in the BRET signal was observed when either Sec14 or PH domains were expressed independently. Because Sec14 and PH domains of NF1 are tightly integrated [24], we conclude that the Sec14/PH module of NF1 forms a novel molecular entity for the specific interaction with Gβγ.

Typically, Gβγ subunits are unable to interact with effector molecules (e.g., NF1) in their inactive state, due to occlusion of the effector-binding interface by the Gα subunits in the heterotrimer complex. Activation of GPCR by agonists promotes binding of GTP to α subunits, leading to dissociation of the heterotrimer and release of the Gβγ subunits. Upon termination of GPCR activation, Gα subunit hydrolyses GTP and then reassociates with Gβγ subunits. Therefore, we examined whether Gβγ-Sec14/PH interaction can be regulated by GPCR activity by measuring real-time changes in the BRET signal upon MORs activation/deactivation (Figure 1K). Stimulation of MORs with increasing concentrations of morphine led to a progressive increase in amplitude of BRET response. Conversely, inactivation of MORs with the antagonist naltrexone rapidly quenched the signal (Figure 1K). Furthermore, the speed of the signal transfer between Gβγ and NF1 ($1/\tau = 0.67 \pm 0.05\ s^{-1}$) matched kinetics of G protein activation and NF1 membrane recruitment (Figure 1B). Dose-response studies revealed a half maximal effective concentration (EC_{50}) value of 40 ± 10 nM for morphine-induced BRET signal between Gβγ and NF1 pair (Figure 1L), which is in close agreement with EC_{50} of G protein activation by MOR studied by GTPγS binding [25]. Notably, the signal transfer was blocked by the Gβγ scavenger GRK3ct, indicating a specific nature of the binding (Figure 1L). A similar blockade was also seen with NF1 dominant-negative construct (Figures S1D–S1F). Finally, overexpression of NF1 in HEK293 cells did not abolish ERK phosphorylation upon activation of MOR yet significantly diminished it (Figures S1G and S1H), again indicating that NF1 is involved in transduction of MOR signals. In summary, these data indicate that Gβγ subunits bind specifically and directly to Sec14/PH module of NF1 and that this interaction is dynamically modulated by changes in the activity of MOR.

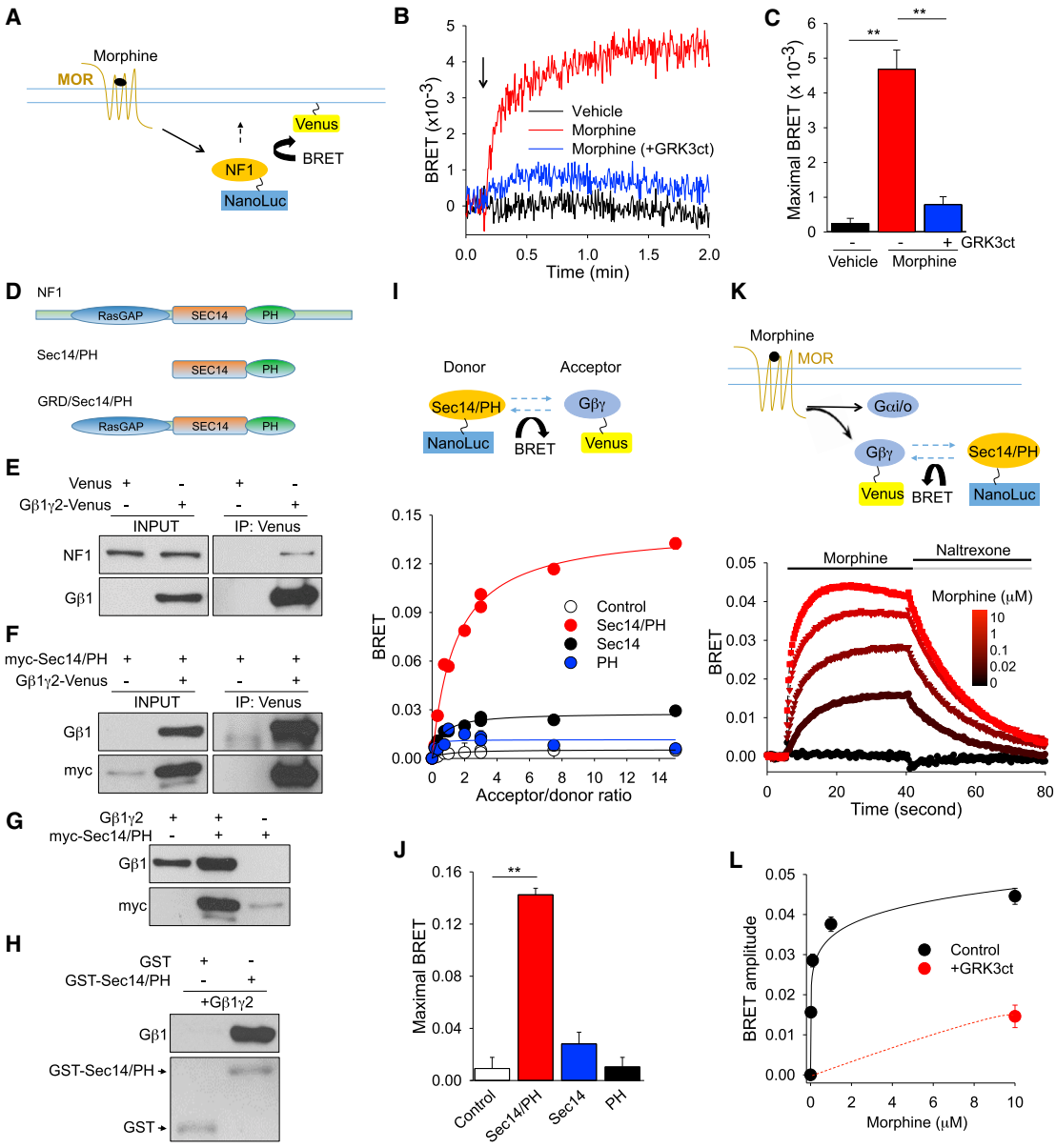

Figure 1. NF1 Is a Novel G Protein Effector Downstream from MORs Activation

(A) Schematic of the assay design to study membrane recruitment of NF1 in response to MOR activation. Association of NanoLuc-tagged NF1 with membrane-targeted Venus is expected to result in BRET signal.

(B) Real-time kinetics of BRET signal change upon NF1 plasma membrane recruitment. Arrow indicates time of morphine application.

(C) Quantification of maximal amplitude of BRET signals from three independent experiments. **$p < 0.01$; one-way ANOVA post hoc Tukey's test.

(D) Schematic representation of NF1 domain composition and truncation mutants used in this study.

(E) Co-immunoprecipitation of endogenous NF1 with overexpressed Gβ1γ2 complex in transfected HEK293T cells.

(F) Co-immunoprecipitation of Sec14/PH module with Gβ1γ2 complex in transfected HEK293T cells.

(G) Mutual stabilization of Sec14/PH module and Gβ1γ2 upon co-expression in HEK293T cells.

(H) Direct interaction between purified recombinant Sec14/PH and Gβ1γ2 proteins studied in pull-down assays.

(I) (Upper) Schematic diagram of BRET strategy to study NF1-Gβγ interaction in living cells. (Lower) Analysis of Gβγ binding to NF1 constructs by titrating ratios of interacting partners is shown.

(J) Quantification of maximal BRET ratios generated by various NF1 constructs from three independent experiments. **$p < 0.01$; one-way ANOVA post hoc Tukey's test.

(K) (Upper) Schematic representation of the BRET assay monitoring interaction between Sec14/PH and Gβγ upon MORs activation and inactivation. (Lower) Real-time kinetics of BRET signal in response to changes in MOR activity is shown.

(L) Quantification of the dose-response relationship of Gβγ-NF1 interaction from three independent experiments. Gβγ scavenger GRK3ct blunted the BRET response between Sec14/PH module and Gβγ.

Data are represented as mean ± SEM. See also Figure S1.

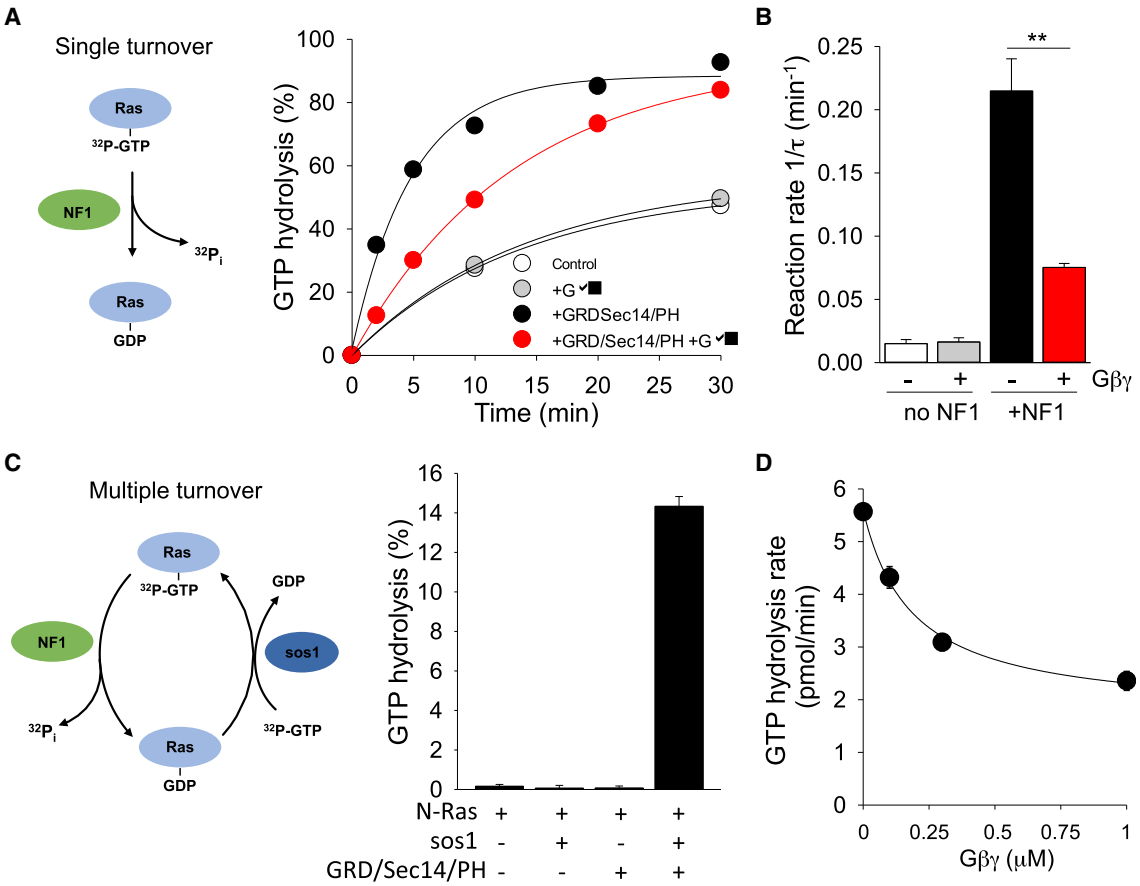

Figure 2. Gβγ Inhibits GAP Activity of NF1

(A) (Left) Diagram of single turnover principle of Ras GTP hydrolysis assay. (Right) Effects of recombinant Gβγ on NF1 fragment (GRD/Sec14/PH)-stimulated GTPase activity of N-Ras are shown.

(B) Quantification of the effect of Gβγ on GTPase activity of NF1.

(C) (Left) Diagram of multiple turnover of Ras GTP hydrolysis assay principle. The assay involves both GAP (NF1) and GEF (sos1). (Right) Both RasGEF and RasGAP are necessary for Ras GTP hydrolysis in the multiple turnover assay.

(D) Gβγ inhibits Ras GTP hydrolysis rate in dose-dependent manner with half maximal inhibitory concentration (IC_{50}) for Gβγ of 0.187 ± 0.044 μM.

Data are represented as mean ± SEM.

Gβγ Inhibits NF1-Mediated Inactivation of Ras

We next analyzed the functional consequences of Gβγ binding to NF1. As a GAP protein, NF1 utilizes its conserved GAP-related domain (GRD) to accelerate GTPase activity of Ras. Interestingly, the GRD module is located in the immediate vicinity of Sec14/PH module (Figure 1D). Thus, we studied the GAP activity of the GRD/Sec14/PH fragment toward Ras in the in vitro system with purified recombinant proteins in the presence or absence of Gβγ (Figure 2). Under single turnover conditions, the addition of the GRD/Sec14/PH module greatly accelerated GTP hydrolysis on Ras. The time constant of the reaction increased from 0.015 ± 0.003 min^{-1} to 0.215 ± 0.025 min^{-1} (Figures 2A and 2B). Gβγ significantly inhibited the NF1's GAP activity but had no effect on the rate of basal GTP hydrolysis by Ras in the absence of NF1.

To obtain further insight into the inhibitory action of Gβγ, we next performed an assay under multiple turnover conditions that more closely reflect the physiological setting. In this assay system, we introduced GEF protein Sos1 for the Ras to undergo multiple activation/deactivation cycles (Figure 2C). Again, Gβγ markedly inhibited acceleration in steady-state Ras GTPase activity mediated by the GRD/Sec14/PH module causing approximately 2.5-fold inhibition (from 5.56 ± 0.13 pmol/min to 2.35 ± 0.17 pmol/min; Figure 2D). This inhibitory effect was dose-dependent and showed saturation. Together, these results indicate that Gβγ binding to NF1 potently inhibits its GAP activity toward Ras.

NF1 Is Necessary for μ-Opioid Receptor Coupling to Ras Activation in Striatal Medium Spiny Neurons

In order to study the role of NF1 in transmission of MOR signals in the native environment, we examined the contribution of NF1 to Ras activation by morphine in cultured striatal MSNs. We monitored Ras activation by utilizing fluorescence lifetime imaging (FLIM)-Forster resonance energy transfer (FRET) approach (Figure 3A), which uses optical sensors to detect changes in Ras activity in real time. Application of morphine resulted in a readily detectable increase in the FLIM-FRET signal in cultured MSNs,

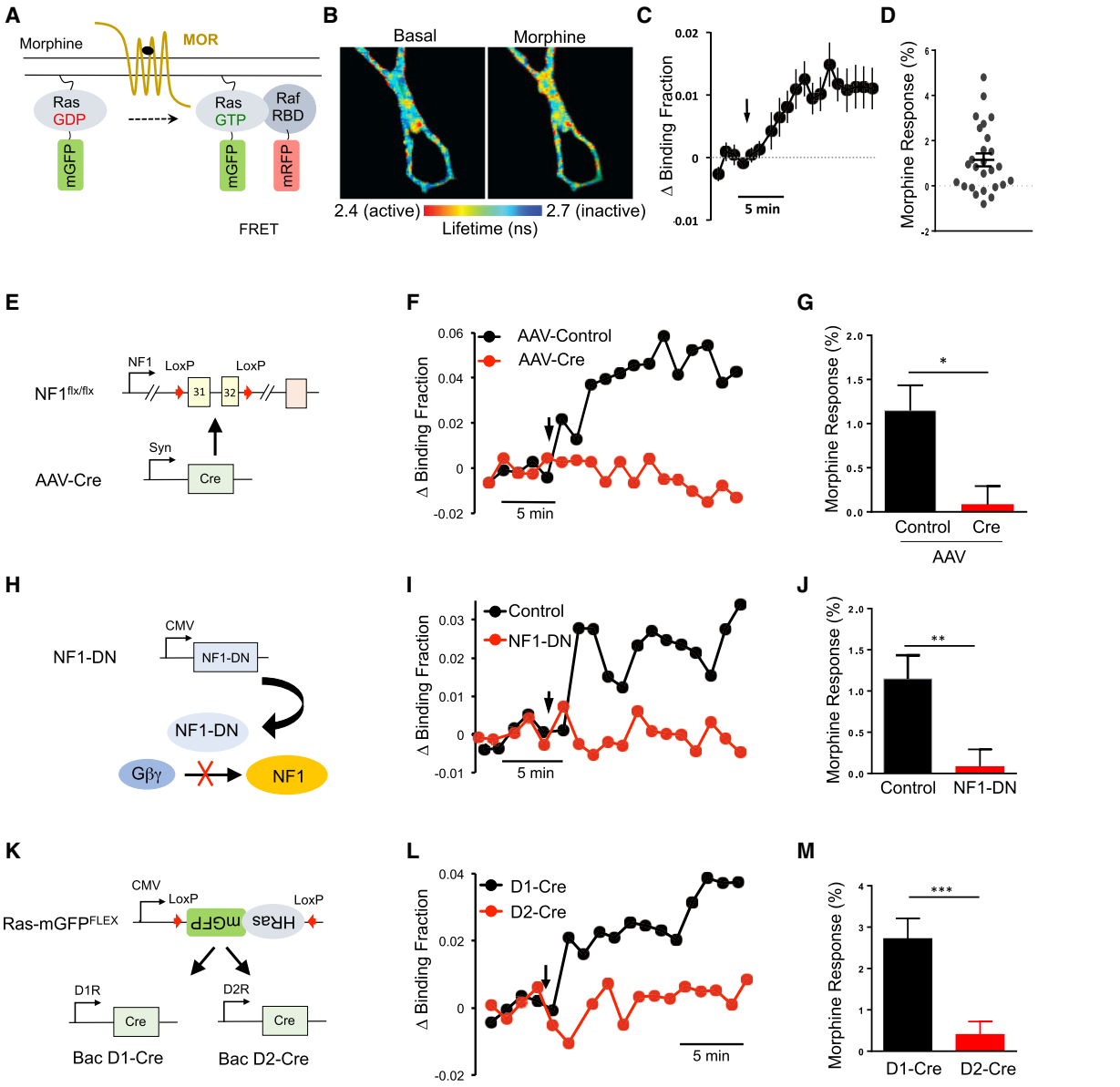

Figure 3. NF1 Is Essential for Ras Activation by MORs in Cultured Striatal MSNs

(A) Schematic of Ras FLIM-FRET sensor. Increase in binding between mGFP-RasGTP and mRFP-Raf-RBD upon Ras activation is measured as a decrease in GFP fluorescence lifetime and quantified as change in binding fraction.

(B) Representative fluorescence lifetime image of striatal MSNs before and 10 min after 10 μM morphine application. Warmer colors indicate decrease in lifetime, which corresponds to higher Ras activity.

(C) Average time course of Ras activation (change in binding fraction) of MSNs in response to 10 μM morphine application (black arrow). Average includes neurons that responded and those that showed no response to morphine.

(D) Morphine-induced Ras activation of individual MSNs.

(E) Schematic of conditional *Nf1* ablation strategy in cultured MSNs. Cultured MSNs from neonatal *Nf1*$^{flx/flx}$ mice were infected with AAV-Cre to induce *Nf1* elimination.

(F) Representative time course of Ras activation (change in binding fraction) in response to morphine application (black arrow) in wild-type (WT) (AAV-control) and *Nf1* cKO (AAV-Cre) MSNs.

(G) Quantification of Ras response to morphine in control and *Nf1* cKO (Cre) cultures. Unpaired t test; *p = 0.02; n = 26 and 15.

(H) Schematic of strategy to prevent Gβγ binding to NF1 by expressing the minimal binding module of NF1 (NF1-DN).

(I) Representative time course of Ras activation (change in binding fraction) in response to morphine application (black arrow) in control and NF1-DN-expressing MSNs.

(J) Quantification of Ras response to morphine in control and NF1-DN-expressing cultures. Unpaired t test; **p = 0.007; n = 19 and 18.

(K) Schematic outlining strategy for expression of Ras sensor in D1R- or D2R-expressing MSNs.

(legend continued on next page)

indicative of Ras activation (Figure 3B). Ras activity rapidly increased and reached a steady-state plateau in ~5 min (Figure 3C). Consistent with the observation that MOR is not expressed in all striatal neurons (Figures S1A and S1B), we found that morphine elicited a significant response in approximately half of neurons (11 out of 26 examined; Figure 3D). Using this system, we first analyzed consequences of NF1 ablation. Infection of cultured striatal neurons from conditional *NF1*$^{flx/flx}$ mice with AAV-Cre (Figure 3E) resulted in a substantial reduction of the NF1 protein expression level compared to cultures treated with the control AAV virus (Figure S2A). Remarkably, we detected no significant Ras activation in response to morphine in cultures where NF1 was deleted by AAV-Cre treatment (Figures 3F and 3G). In contrast, treatment of MSNs with AAV-Cre did not significantly affect the response to BDNF stimulation (Figures S2B–S2D), which is known to transduce the signal by activating Ras through GEF proteins. This indicates that deletion of NF1 specifically abolished coupling of MOR to Ras, while preserving the ability of Ras to be activated by receptor tyrosine kinases.

To further test specificity of the observed effects, we used a dominant-negative strategy to selectively disrupt Gβγ binding to NF1 (Figure 3H). Introduction of the dominant-negative NF1 construct that prevents Gβγ binding to NF1 and disrupts signal transfer from the MOR to NF1 (Figures S1C–S1F) blocked morphine-induced Ras activation (Figures 3I and 3J). This manipulation, once again, had no effect on Ras activation in response to BDNF application (Figure S2E). These results suggest that activation of Ras in MSN neurons in response to morphine specifically requires Gβγ interaction with NF1.

We next addressed the cell specificity of MOR coupling to Ras. Striatal MSNs form two molecularly distinct populations that project to different output regions and distinctly impact behavioral responses: D1-dopamine-receptor-expressing neurons of the direct pathway (dMSN) and D2-dopamine-receptor-expressing (D2R) neurons of the indirect pathway (iMSN) [2]. Consistent with its broad distribution in the striatum, NF1 was significantly co-expressed with both D1R and D2R (Figure S2F). To assess MOR coupling to Ras in each of these populations, we delivered an inverted Ras-sensor donor construct flanked with inverted loxP sites to cultured striatal neurons from *D1-Cre* or *D2-Cre* mice (Figure 3K). Using this strategy, Ras sensors are expressed only in cells containing Cre recombinase, allowing Ras activity to be monitored selectively in striatal neurons expressing either D1R or D2R. Application of morphine to striatal cultures from *D1-Cre* mice elicited robust FLIM-FRET signal changes, indicating Ras activation (Figures 3L and 3M) from nearly all neurons examined (13 out of 15). In contrast, we detected no Ras activation induced by morphine application in cultures from *D2-Cre* mice. Importantly, responses to BDNF in both cultures were not significantly different from each other (Figure S2G), indicating that the conditional imaging strategy can successfully report Ras activation in both MSN populations, if it occurs. Together, these results demonstrate an essential requirement of NF1 for coupling MORs to Ras activation in striatal dMSN neurons.

NF1 Mediates Opioid Signaling to Ras-Akt-mTOR in the Striatum

We next determined the in vivo relevance of NF1 for opioid-mediated signaling in the striatum. Striatal-specific inactivation of NF1 (*Nf1* cKO) was achieved by crossing conditional *Nf1*$^{flx/flx}$ mice with the *Rgs9-Cre* driver line, which expresses Cre recombinase selectively in striatal neurons (Figure 4A). Morphological analysis revealed that *Nf1* cKO mice had normal striatal architecture with no evidence of degenerative changes (Figure 4B). Immunoblotting analysis showed a readily detectible reduction in the levels of NF1 protein (Figures 4C and 4D). As expected from its function as Ras GAP, we detected an elevation in the levels of active Ras in the striatum of *Nf1* cKO mice (Figures 4C and 4D). Consistent with these changes in the baseline activity of Ras, we found a significant elevation in phosphorylation of ERK, a downstream target of Ras (Figures 4C, 4D, and S3A). Interestingly, we found the basal activation of Akt, another kinase regulated by Ras signaling to be reduced in *Nf1* cKO striatum tissue (Figures 4C, 4D, and S3A). Whereas we did not investigate the mechanisms behind this adaptation, we think that it is likely related to known feedback inhibition by activated ERK [26].

To study the role of NF1 in MOR-mediated signaling, we focused on two separate signaling branches downstream from Ras: Raf-ERK and Akt-mTOR/GSK3β (Figure 4E). Administration of morphine (20 mg/kg for 1 hr) resulted in significant elevation of active Ras (Ras-GTP) in the striatum of control mice, but not in *Nf1* cKO mice (Figures 4F and 4G). Accordingly, morphine injections increased phosphorylation of Akt, GSK3β, and mTOR in control mice but completely failed to do so in the absence of NF1 (Figures 4F and 4G). In agreement with previous reports [21], we did not detect significant ERK activation in response to morphine in either control or *Nf1* cKO mice, suggesting that MOR-mediated activation of Ras in the striatum primarily signals via the Akt-mTOR/GSK3β pathway, with NF1 playing a key role in this process. To test whether the lack of kinase pathway by morphine in *Nf1* cKO mice could be explained by the signaling occlusion due to elevated basal levels of active Ras, we stereotaxically injected BDNF in the striatum. This treatment resulted in significant Ras activation as well as phosphorylation of AKT, ERK, and S6 in both genotypes, indicating that elimination of NF1 does not completely prevent further regulation of Ras-signaling pathways (Figure S3B).

Ablation of NF1 in the Striatum Blunts Behavioral Responses to Morphine

We next examined the effects of striatal NF1 ablation on opioid-induced behaviors. Open field test revealed that *Nf1* cKO mice had overall normal behavioral reactions, including spontaneous locomotor activity, habituation, anxiety, and motor coordination (Figures S4A–S4C). Administration of morphine produced significantly lower psychomotor activation in *Nf1* cKO mice (Figures

(L) Representative time course of Ras activation (change in binding fraction) in response to morphine application (black arrow) in D1R- and D2R-expressing MSNs.

(M) Quantification of Ras response to morphine in D1R- and D2R-expressing MSNs. Unpaired t test; **p = 0.007; n = 13 and 15.

Data are represented as mean ± SEM. See also Figure S2.

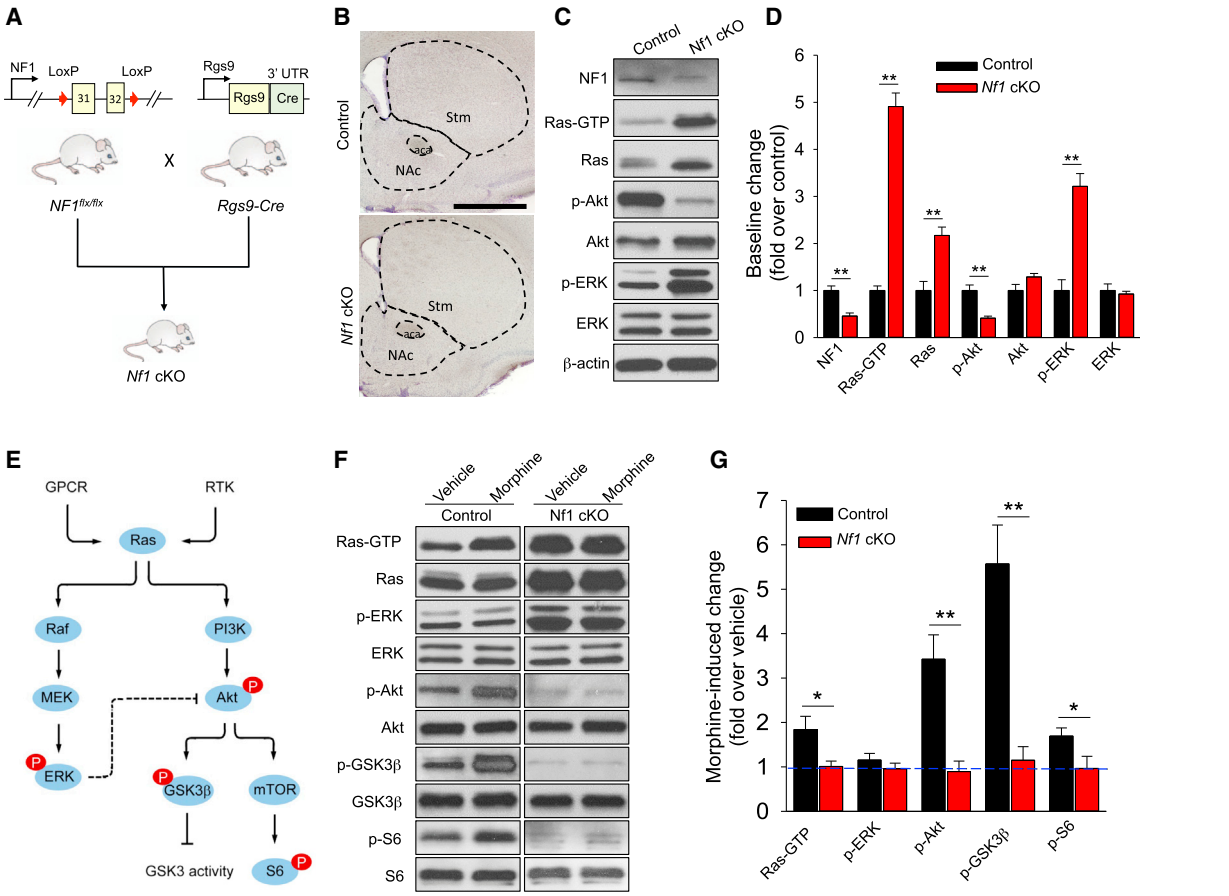

Figure 4. Striatal NF1 Is Essential for Morphine-Induced Ras and Its Downstream Signaling Cascade Activation

(A) Generation of striatal-specific *Nf1* knockout mice (*Nf1* cKO) by crossing conditional $NF1^{flx/flx}$ line with MSNs-specific *Rgs9-Cre* line.

(B) Representative images of Nissl-stained coronal brain sections from control and *Nf1* cKO mice. aca, anterior part of anterior commissure; NAc, nucleus accumbens; Stm, striatum (scale bar, 1 mm). We found average volumes of both dorsal striatum (16.4 ± 0.8 mm^3 in *Nf1* cKO versus 17.2 ± 0.3 mm^3 in control littermates; n = 4 mice) and nucleus accumbens (1.4 ± 0.1 mm^3 in *Nf1* cKO versus 1.3 ± 0.1 mm^3 in control littermates; n = 4 mice) to be unaffected by NF1 deletion.

(C) Impact of NF1 elimination on baseline Ras activation and signaling to downstream kinase pathways in striatum.

(D) Quantification of western blot data with activities normalized to samples from control mice. Data are represented as mean ± SEM. **$p < 0.01$; Student's t test.

(E) Schematic representation of Ras-ERK and Ras-Akt signaling. Ras is activated in response to both GPCRs and receptor tyrosine kinases (RTKs), which in turn is able to activate both Raf/MEK/ERK and PI3K/Akt pathways. Activated Akt can further modulate GSK3 and mTOR activity. High level of ERK activity can result in decreased activity of Akt through cross-talk.

(F) Morphine-induced activation of Ras and its downstream pathway in striatum studied by western blotting. Mice were injected with 20 mg/kg morphine (subcutaneously [s.c.]) or saline, and their NAc regions were dissected 60 min after for active Ras pull-down as well as western blot analysis.

(G) Quantification of western blot data with activities normalized to vehicle-treated control of the same genotype. *$p < 0.05$; **$p < 0.01$; n = 3 mice per each treatment; Student's t test.

See also Figure S3.

5A and 5B). Interestingly, the onset, duration, and recovery of mice from psychomotor activation produced by morphine action were similar between genotypes, yet the effect of morphine in *Nf1* cKO mice plateaued, much below the level seen in control mice (Figures 5A and 5B). We found no effect of NF1 ablation on morphine analgesia or analgesic tolerance (Figure S4D) despite a demonstrated role of neurons where RGS9-Cre driver is active in these processes [27].

Because striatum plays a central role in mediating the reinforcing effects of opioids, we next probed the contribution of striatal NF1 ablation in reward-related behaviors. In the conditioned place preference (CPP) paradigm, injection of 7.5 mg/kg morphine caused a significant increase in time spent in the drug-paired side in both *Nf1* cKO mice and their control littermates (Figure 6A). However, the effect was significantly less pronounced in mice lacking NF1. This difference between genotypes was eliminated at a higher dose of morphine (20 mg/kg), suggesting that lack of NF1 decreases sensitivity of morphine reward. We then assessed the selective contribution of MOR signaling via NF1 to the observed effect. This was achieved by injecting an AAV virus containing inverted sequence of NF1-DN dominant-negative construct to prevent Gβγ binding to NF1 in the nucleus accumbens (NAc) of *Rgs9-Cre* mice, limiting the effects to the striatal MSN neurons (Figure 6B). Again,

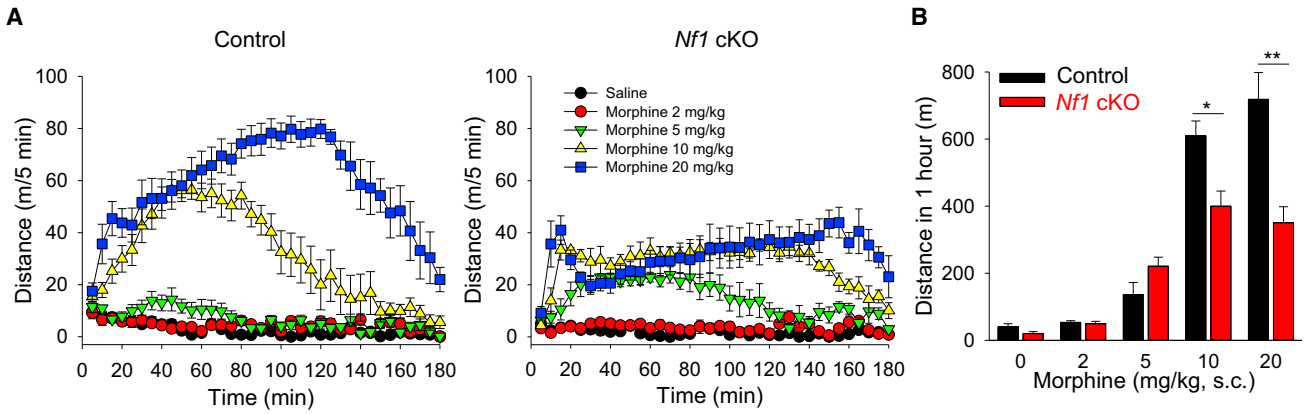

Figure 5. Striatal NF1 Regulates Psychomotor Responses to Morphine

(A) The effect of morphine administration on locomotor activity in control (left) and *Nf1* cKO (right) mice in the open field task. Mice received saline or increasing doses of morphine (2, 5, 10, and 20 mg/kg, s.c.) and were immediately placed in the activity-recording chamber.

(B) Quantification of cumulative distance traveled in open–field chamber during 20–80 min following vehicle or morphine treatment. NF1 ablation in striatum results in blunted morphine-induced psychomotor activation. *$p < 0.05$; **$p < 0.01$; two-way ANOVA post hoc Tukey's test ($n = 8$ mice per each group).

See also Figure S4.

antagonizing Gβγ-NF1 interaction diminished sensitivity of mice to place-preference-inducing effects of morphine, phenocopying the effects of *Nf1* ablation.

Next, we investigated reinforcing properties of morphine in a morphine self-administration paradigm, which models drug-seeking and taking behavior. Initially, mice were trained in a two-lever operant task with food reward (Figure S4E). Whereas both genotypes learned the task to the set criteria, it took considerably longer for *Nf1* cKO mice to establish similar level of lever pressing. Once response to food reinforcement was established, mice were assessed for lever pressing that resulted in morphine infusions (Figure 6C). Both genotypes readily self-administered morphine at a dose of 0.3 mg/kg/infusion; however, *Nf1* cKO mice exhibited a dramatically decreased number of active lever presses, with no change to inactive lever pressing (Figure 6C). This experiment demonstrates that *Nf1* cKO mice have a lower sensitivity to reinforcing effects of morphine. Analysis of the dose-response relationship revealed that *Nf1* cKO mice earned a lower number of morphine infusions compared to control littermates at the doses of 0.3 and 0.6 mg/kg/infusion (Figures 6D and S4F). Interestingly, whereas control mice responded with decreased morphine intake at a higher dose (1 mg/kg/session) and showed typical inverted U-shaped dependence, *Nf1* cKO mice continued to press even more, earning a greater number of rewards (Figure 6D). Both genotypes showed a similar extinction profile upon substitution of morphine with saline, further supporting the conclusion that differences in lever-pressing behavior were related to differences in reinforcing effects of morphine rather than in habitual behaviors. Together, these observations indicate that NF1 is involved in setting the behavioral sensitivity of mice to the rewarding effects of morphine.

DISCUSSION

One of the main results of this study is the demonstration of a novel signaling mechanism for transmitting GPCRs activation to positive regulation of kinase-signaling networks (Figure 7). On the basis of our findings, we propose that NF1 is a direct G protein effector. Inhibition of its Ras GAP activity by Gβγ subunits released upon activation of opioid receptors in striatal neurons resulted in activation of small GTPase Ras. Elimination of NF1 led to elevation of baseline Ras activity and abolished the ability of opioid receptors to regulate Ras activation. This deficit in signal propagation selectively affected responses mediated by the heterotrimeric G proteins and did not influence signaling via receptor tyrosine kinases that activate Ras directly.

Activation of Ras by GPCRs has become an accepted paradigm in cellular signaling. A large number of mechanisms have been proposed to explain how GPCRs signal to Ras (see [28, 29] for review). A majority of the demonstrated mechanisms involve multiple steps and have been described for non-neuronal cell lines. Perhaps the most direct pathway occurs in epithelial cells and involves positive regulation of the Ras exchange factor Ras-GRF1 by Gβγ in a phosphorylation-dependent manner [9], although there is evidence for Gβγ binding to several GEFs for small GTPases [22, 30] as well as some GAPs, e.g., p120Ras-GAP [31]. To the best of our knowledge, however, this work for the first time identified a mechanism for GPCR-mediated activation of Ras in native neuronal cells, making NF1 the first reported GAP for the small GTPases regulated by GPCR signaling. Remarkably, we found that this is the dominant signaling transfer mechanism in the striatal neurons, as the elimination of NF1 completely prevented coupling of opioid receptors to Ras despite multiple potential pathways described in non-neuronal cell types.

The role of NF1 in neuronal function is a subject of intense investigation, largely because mutations in *NF1* cause neurofibromatosis, a disease with prominent neuropsychiatric manifestations that include learning and memory issues, social difficulties, and delays in the acquisition of motor and idiopathic pain [32]. Whereas there has been great progress linking cognitive deficits associated with NF1 deficiency to hippocampal function [33], the broad range of the neuropsychiatric features suggest that NF1 is involved in controlling neuronal functions in

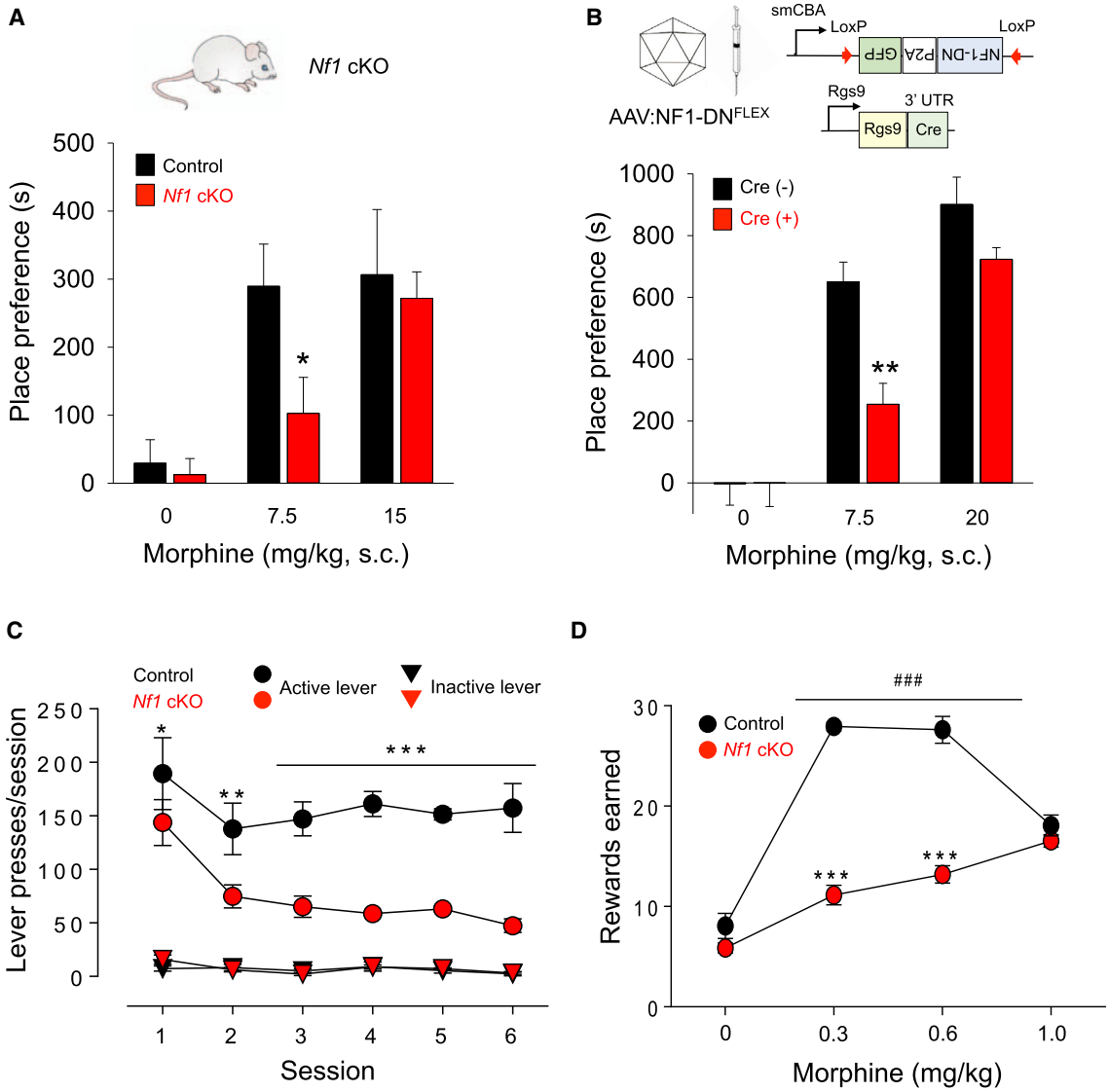

Figure 6. Disruption of MOR Signaling via NF1 in the Striatum Decreases Sensitivity to Morphine Reward

(A) Effect of striatal-specific deletion of NF1 (*Nf1* cKO mice) on mouse performance in conditioned place preference (CPP) task. Mice were administered either saline (0 mg/kg morphine) or various concentrations of morphine as indicated. Place-preference scores are calculated as the time difference during post-conditioning between drug-paired side versus saline-paired side. *$p < 0.05$ in comparison between genotypes two-way ANOVA post hoc Tukey's test ($n = 6–10$ each group).

(B) Effect of disrupting Gβγ-NF1 interaction in the nucleus accumbens (NAc) on morphine CPP. (Upper) Schematics of the conditional dominant-negative construct (AAV-NF1-DN^{FLEX}) and its viral delivery into NAc of *Rgs9-Cre* mice are shown. (Lower) Performance of mice in the CPP task is shown. Mice were administered either saline or various concentrations of morphine as indicated. AAV-mediated expression of a dominant-negative NF1 construct that prevents Gβγ-NF1 interaction decreases sensitivity of mice to rewarding effects of morphine. The same AAV-NF1-DN^{FLEX} virus was injected into either *Rgs9-Cre*(+) mice or their control littermates *Rgs9-Cre*(−). CPP experiments were conducted as in (A). **$p < 0.01$ in comparison between genotypes two-way ANOVA post hoc Tukey's test ($n = 5–6$ each group).

(C) Animal performance in morphine self-administration task. Lever presses per session are plotted. Active (0.3 mg/kg/infusion) versus inactive levers showed significant ($p < 0.01$ and $p < 0.0001$) difference with both genotypes and within criteria. Genotype versus session ($n = 5$ per group) interaction $p = 0.005$; genotype $p < 0.0001$; session $p < 0.0001$. Data are expressed as mean ± SEM. *$p < 0.05$; **$p < 0.01$; ***$p < 0.001$ genotype comparison per session; two-way ANOVA followed by Bonferroni test.

(D) Dose-response dependence of drug taking in the self-administration task. Genotype versus dose ($n = 5$ per group) interaction $p < 0.0001$; genotype $p < 0.0001$; dose $p < 0.0001$. Data are expressed as mean ± SEM. ***$p < 0.001$ genotype comparison; $^{###}p < 0.001$ compared to saline for both genotypes; two-way ANOVA with Bonferroni test.

other brain regions as well. Among these, the involvement of striatal circuits has been suggested [34, 35]. The results of our study reveal that NF1 plays an essential role in the processing neurotransmitter signals in the striatal medium spiny neurons. Acting primarily in D1-receptor-expressing direct pathway neurons, NF1 plays an essential role in linking MOR to Ras

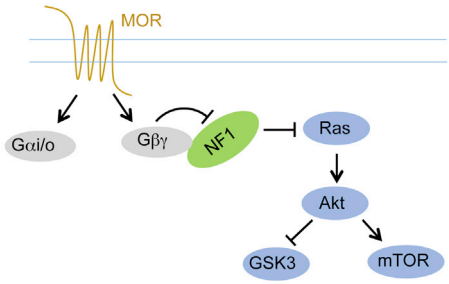

Figure 7. Proposed Model for the Role of NF1 in Mediating MOR Signaling to Ras

NF1 is a novel Gβγ effector downstream from MORs activation and is essential for MORs-induced Ras pathway activation in MSNs.

activation. We found that this NF1 function was necessary for achieving full efficacy of behavioral responses to morphine, establishing it as a key player in controlling opioid effects in the striatum. Interestingly, we find that NF1 plays a critical role in producing rewarding and motivational effects of morphine administration with no impact on morphine-mediated analgesia.

We think that effect of NF1 elimination on behavior and signaling in striatal neurons is unlikely to be limited to blockade of MOR signaling to Ras. Loss of NF1 also results in significant elevation of basal activation of Ras and downstream pERK pathway with concurrent inhibition of basal AKT-mTOR signaling. This effect is expected from the activity of NF1 as a Ras GAP and consistent with similar observations in other cells [36, 37]. Although these changes in baselines were substantial, they did not reach the saturation, and stimulation of receptor tyrosine kinase receptors by BDNF led to further augmentation of Ras activation, indicating that, even if signaling occlusion occurs, it is not complete. Nevertheless, these alterations in baselines of several signaling molecules may contribute to the changes in responses to morphine brought about by NF1 deletion. Furthermore, other second-messenger cascades and receptor systems involved in shaping complex behavioral response to a drug may be affected and thus be also contributing to the observed phenotypes. Regardless of the exact contributions of baseline versus receptor-mediated signaling through Ras pathways, our findings clearly establish the key role of NF1 in the process.

Given that the endogenous opioid system plays a role in the actions of many abused drugs, including alcohol [38], we think it is likely that the MOR-NF1-Ras pathway in the striatum may be involved in setting the incentive salience value of incoming signals and thus contributing to controlling addictive properties of drugs in general. In agreement with this idea, mutations in NF1 have recently been associated with predisposition to alcohol addiction, and NF1 haploinsufficiency protected mice from developing dependence [39]. Furthermore, we found that NF1 ablation also diminished acquisition of lever-pressing behavior when food was used as a reinforcer. Although this may be related to deficits in the instrumental learning, which striatum is involved in, we think that it is equally plausible that this may also suggest a role of NF1 in controlling endogenous opioid system, as it has been shown to play a prominent role in regulating food reward [40]. Together, our observations introduce NF1 as a key regulator of opioid signaling and reward processing in the striatum.

Activation of Ras is one of the central hubs in cellular signaling, which can engage a variety of the signaling pathways downstream. From this perspective, it is interesting that, in striatal neurons, activation of Ras-regulated kinase pathways by MOR is functionally biased. In agreement with previous reports [21, 41, 42], we found that morphine did not increase ERK1/2 phosphorylation despite robust activation of Ras. Instead, regulation of the Akt signaling branch by morphine was clearly evident. At the same time, elimination of NF1 affected basal levels of both Akt-mTOR and ERK1/2 activation, suggesting that this bias likely originates at the level of the receptor. Indeed, MOR has been shown to be capable of activating ERK1/2 in striatal neurons when stimulated by a different opioid agonist fentanyl in a manner dependent on GRK3/β-arrestin [41]. This example serves to reinforce the ligand-dependent nature of opioid receptor signaling that is becoming an increasingly accepted model of GPCR signaling [43, 44]. Nevertheless, from the perspective of G-protein-mediated transmission downstream from MOR, Ras signaling to Akt-mTOR/GSK3β seems to be the dominant pathway regulated by NF1. Another interesting observation is that, in striatal neurons, the homeostatic set point for the regulation of basal Akt-mTOR/GSK3β activity appears to differ from that seen in other cells. Whereas the elimination of NF1 in astrocytes results in Akt-mTOR hyperactivation [45], we observed hypoactivity of Akt-mTOR signaling in striatal tissue lacking NF1. We think that this downregulation of basal Akt signaling results from a negative feedback imposed by excessive ERK1/2 activity, which was reported to occur in human breast cancer cells [26, 46]. The exact molecular mechanisms of this ERK1/2-Akt-signaling cross-talk are not well understood, and determining the role of NF1 in this process along with its implication for neuronal physiology appears to be an interesting direction for future studies.

The loss of the receptor-mediated activation of Ras in the striatal neurons that we report in this study calls for revisiting the current paradigm that views upregulation of Ras signaling as a primary cause of neurofibromatosis [47, 48]. This rationale provides a theoretical basis for Ras inhibition as a therapeutic strategy for neurofibromatosis treatment. However, clinical trials using statins that reduce Ras activation have had mixed success in ameliorating neuropsychiatric symptoms of the disease [49, 50]. Whereas our results confirm the well-documented increase in basal levels of active Ras associated with NF1 dysfunction, they additionally reveal that the signal-regulated Ras activation (e.g., through MOR activation) is abolished. Thus, insufficiency of signaling through Ras may contribute to some of the neuropsychiatric manifestations seen in type 1 neurofibromatosis. From this perspective, NF1-mediated opioid signaling to Ras in the striatum may prove helpful for understanding related aspects of the disease, such as goal-directed learning difficulties, as well as for exploring opioid receptors as possible therapeutic targets for neurofibromatosis. Whereas our research primarily focused on examining the role of NF1 in the regulation of opioid receptor signaling specifically in the striatal neurons, we think that these observations could be broadly applicable to other cells and GPCRs where NF1 plays a dominant role in controlling basal Ras activation.

EXPERIMENTAL PROCEDURES

Bioluminescence Resonance Energy Transfer Assay

A new version of NanoBRET was performed to visualize the interaction between the NanoLuc-tagged energy donor and the Venus-tagged energy acceptor. NanoBRET assays were applied to examine NF1 membrane recruitment, the specific interaction between Sec14/PH and Gβγ, and the real-time interaction between Sec4/PH and Gβγ upon GPCR activation/inactivation.

Ras GTP Hydrolysis Assay

Ras GTPase activity was examined in both single and multiple turnover Ras GTP hydrolysis assays using purified recombinant proteins. GTP hydrolysis was examined by measuring the generation of inorganic phosphate $^{32}P_i$ released from hydrolyzed [γ-^{32}P]GTP by activated charcoal assay.

Ras Activity Measured by Two-Photon Fluorescence Lifetime Imaging Assay

Cultured striatal neurons were transfected with the FLIM-FRET Ras sensors mEGFP-HRas and mRFP-RBD-mRFP and imaged under a two-photon microscope. Fluorescence lifetime images were acquired using time-correlated, single-photon counting, and Ras activation was quantified as fraction of mEGFP-HRas bound to mRFP-RBD-mRFP through fitting the fluorescence decay curve.

Animals

All procedures were approved by the Institutional Animal Care and Use Committee at The Scripps Research Institute. Homozygous *Nf1*$^{flx/flx}$ mice were bred against heterozygous *Rgs9-Cre* mice to generate striatal specific NF1 conditional knockout (*Nf1* cKO) mice. Mice of either sex were used.

Statistics

All data are presented as the mean ± SEM. Two sample comparisons were made using the Student's t test. All comparisons relating test to control data from littermate animals were analyzed statistically using two-way ANOVA.

Additional details can be found in the Supplemental Experimental Procedures.

SUPPLEMENTAL INFORMATION

Supplemental Information includes four figures and Supplemental Experimental Procedures and can be found with this article online at http://dx.doi.org/10.1016/j.cub.2016.09.010.

AUTHOR CONTRIBUTIONS

K.X. performed all biochemical experiments described in the paper, including protein-protein interaction assays, BRET studies, and in vitro GAP assays; he also performed behavioral studies, analyzed data, and wrote the manuscript. S.L.B. and S.E.B. designed and generated recombinant AAV vectors. L.A.C. performed FLIM-FRET experiments in striatal neurons and analyzed the data. C.O. performed in situ hybridization experiments. B.S.M. conducted BRET, coIP studies, and experiments involving D1-Cre- and D2-Cre-cultured neurons. L.P.S. designed and executed hot-plate behavioral experiments. C.-C.S. and B.X. performed morphological analysis of striatum and analyzed the data. Y.L. provided the RGS9-Cre mouse strain. M.T.D. and R.G.S. designed and executed self-administration experiments. M.T.D. performed viral injections and some CPP experiments. R.Y. designed FLIM-FRET experiments and analyzed the data. K.A.M. designed the study, analyzed data, and wrote the manuscript.

ACKNOWLEDGMENTS

We wish to thank Ms. Natalia Martemyanova for producing and maintaining mice examined in this study and Maxwell Kassel for technical assistance with some of the experiments. This work was supported by NIH grants DA036082 (to K.A.M.), MH080047 (to R.Y.), MH101954 (to L.A.C.), NS82244 (to Y.L.), NS073930 (to B.X.), and EY024280 (to S.E.B.) and Department of Defense CDMRP grant W81XWH-14-1-0074 (to K.A.M.).

Received: April 22, 2016
Revised: August 24, 2016
Accepted: September 7, 2016
Published: October 20, 2016

REFERENCES

1. Graybiel, A.M. (2000). The basal ganglia. Curr. Biol. *10*, R509–R511.
2. Kreitzer, A.C., and Malenka, R.C. (2008). Striatal plasticity and basal ganglia circuit function. Neuron *60*, 543–554.
3. Xie, K., and Martemyanov, K.A. (2011). Control of striatal signaling by g protein regulators. Front. Neuroanat. *5*, 49.
4. Pierce, K.L., Premont, R.T., and Lefkowitz, R.J. (2002). Seven-transmembrane receptors. Nat. Rev. Mol. Cell Biol. *3*, 639–650.
5. Fasano, S., and Brambilla, R. (2011). Ras-ERK signaling in behavior: old questions and new perspectives. Front. Behav. Neurosci. *5*, 79.
6. Thomas, G.M., and Huganir, R.L. (2004). MAPK cascade signalling and synaptic plasticity. Nat. Rev. Neurosci. *5*, 173–183.
7. Crespo, P., Xu, N., Simonds, W.F., and Gutkind, J.S. (1994). Ras-dependent activation of MAP kinase pathway mediated by G-protein beta gamma subunits. Nature *369*, 418–420.
8. Koch, W.J., Hawes, B.E., Allen, L.F., and Lefkowitz, R.J. (1994). Direct evidence that Gi-coupled receptor stimulation of mitogen-activated protein kinase is mediated by G beta gamma activation of p21ras. Proc. Natl. Acad. Sci. USA *91*, 12706–12710.
9. Mattingly, R.R., and Macara, I.G. (1996). Phosphorylation-dependent activation of the Ras-GRF/CDC25Mm exchange factor by muscarinic receptors and G-protein beta gamma subunits. Nature *382*, 268–272.
10. Bos, J.L., Rehmann, H., and Wittinghofer, A. (2007). GEFs and GAPs: critical elements in the control of small G proteins. Cell *129*, 865–877.
11. Le Merrer, J., Becker, J.A., Befort, K., and Kieffer, B.L. (2009). Reward processing by the opioid system in the brain. Physiol. Rev. *89*, 1379–1412.
12. Nestler, E.J. (2001). Molecular basis of long-term plasticity underlying addiction. Nat. Rev. Neurosci. *2*, 119–128.
13. Law, P.Y., Wong, Y.H., and Loh, H.H. (2000). Molecular mechanisms and regulation of opioid receptor signaling. Annu. Rev. Pharmacol. Toxicol. *40*, 389–430.
14. Mansour, A., Fox, C.A., Burke, S., Meng, F., Thompson, R.C., Akil, H., and Watson, S.J. (1994). Mu, delta, and kappa opioid receptor mRNA expression in the rat CNS: an in situ hybridization study. J. Comp. Neurol. *350*, 412–438.
15. Oude Ophuis, R.J., Boender, A.J., van Rozen, A.J., and Adan, R.A. (2014). Cannabinoid, melanocortin and opioid receptor expression on DRD1 and DRD2 subpopulations in rat striatum. Front. Neuroanat. *8*, 14.
16. Cui, Y., Ostlund, S.B., James, A.S., Park, C.S., Ge, W., Roberts, K.W., Mittal, N., Murphy, N.P., Cepeda, C., Kieffer, B.L., et al. (2014). Targeted expression of μ-opioid receptors in a subset of striatal direct-pathway neurons restores opiate reward. Nat. Neurosci. *17*, 254–261.
17. Robinson, T.E., and Kolb, B. (1999). Morphine alters the structure of neurons in the nucleus accumbens and neocortex of rats. Synapse *33*, 160–162.
18. Russo, S.J., Dietz, D.M., Dumitriu, D., Morrison, J.H., Malenka, R.C., and Nestler, E.J. (2010). The addicted synapse: mechanisms of synaptic and structural plasticity in nucleus accumbens. Trends Neurosci. *33*, 267–276.
19. Ye, X., and Carew, T.J. (2010). Small G protein signaling in neuronal plasticity and memory formation: the specific role of ras family proteins. Neuron *68*, 340–361.
20. Mazei-Robison, M.S., Koo, J.W., Friedman, A.K., Lansink, C.S., Robison, A.J., Vinish, M., Krishnan, V., Kim, S., Siuta, M.A., Galli, A., et al. (2011). Role for mTOR signaling and neuronal activity in morphine-induced adaptations in ventral tegmental area dopamine neurons. Neuron *72*, 977–990.
21. Muller, D.L., and Unterwald, E.M. (2004). In vivo regulation of extracellular signal-regulated protein kinase (ERK) and protein kinase B (Akt)

phosphorylation by acute and chronic morphine. J. Pharmacol. Exp. Ther. *310*, 774–782.

22. Inglese, J., Koch, W.J., Touhara, K., and Lefkowitz, R.J. (1995). G beta gamma interactions with PH domains and Ras-MAPK signaling pathways. Trends Biochem. Sci. *20*, 151–156.
23. Nishida, K., Kaziro, Y., and Satoh, T. (1999). Association of the proto-oncogene product dbl with G protein betagamma subunits. FEBS Lett. *459*, 186–190.
24. D'Angelo, I., Welti, S., Bonneau, F., and Scheffzek, K. (2006). A novel bipartite phospholipid-binding module in the neurofibromatosis type 1 protein. EMBO Rep. *7*, 174–179.
25. Xu, H., Wang, X., Partilla, J.S., Bishop-Mathis, K., Benaderet, T.S., Dersch, C.M., Simpson, D.S., Prisinzano, T.E., and Rothman, R.B. (2008). Differential effects of opioid agonists on G protein expression in CHO cells expressing cloned human opioid receptors. Brain Res. Bull. *77*, 49–54.
26. Klos, K.S., Wyszomierski, S.L., Sun, M., Tan, M., Zhou, X., Li, P., Yang, W., Yin, G., Hittelman, W.N., and Yu, D. (2006). ErbB2 increases vascular endothelial growth factor protein synthesis via activation of mammalian target of rapamycin/p70S6K leading to increased angiogenesis and spontaneous metastasis of human breast cancer cells. Cancer Res. *66*, 2028–2037.
27. Zachariou, V., Georgescu, D., Sanchez, N., Rahman, Z., DiLeone, R., Berton, O., Neve, R.L., Sim-Selley, L.J., Selley, D.E., Gold, S.J., et al. (2003). Essential role for RGS9 in opiate action. Proc. Natl. Acad. Sci. USA *100*, 13656–13661.
28. Gutkind, J.S. (2000). Regulation of mitogen-activated protein kinase signaling networks by G protein-coupled receptors. Sci. STKE *2000*, re1.
29. Wetzker, R., and Böhmer, F.D. (2003). Transactivation joins multiple tracks to the ERK/MAPK cascade. Nat. Rev. Mol. Cell Biol. *4*, 651–657.
30. Niu, J., Profirovic, J., Pan, H., Vaiskunaite, R., and Voyno-Yasenetskaya, T. (2003). G Protein betagamma subunits stimulate p114RhoGEF, a guanine nucleotide exchange factor for RhoA and Rac1: regulation of cell shape and reactive oxygen species production. Circ. Res. *93*, 848–856.
31. Xu, N., Coso, O., Mahadevan, D., De Blasi, A., Goldsmith, P.K., Simonds, W.F., and Gutkind, J.S. (1996). The PH domain of Ras-GAP is sufficient for in vitro binding to beta gamma subunits of heterotrimeric G proteins. Cell. Mol. Neurobiol. *16*, 51–59.
32. Créange, A., Zeller, J., Rostaing-Rigattieri, S., Brugières, P., Degos, J.D., Revuz, J., and Wolkenstein, P. (1999). Neurological complications of neurofibromatosis type 1 in adulthood. Brain *122*, 473–481.
33. Costa, R.M., Federov, N.B., Kogan, J.H., Murphy, G.G., Stern, J., Ohno, M., Kucherlapati, R., Jacks, T., and Silva, A.J. (2002). Mechanism for the learning deficits in a mouse model of neurofibromatosis type 1. Nature *415*, 526–530.
34. Shilyansky, C., Karlsgodt, K.H., Cummings, D.M., Sidiropoulou, K., Hardt, M., James, A.S., Ehninger, D., Bearden, C.E., Poirazi, P., Jentsch, J.D., et al. (2010). Neurofibromin regulates corticostriatal inhibitory networks during working memory performance. Proc. Natl. Acad. Sci. USA *107*, 13141–13146.
35. Brown, J.A., Xu, J., Diggs-Andrews, K.A., Wozniak, D.F., Mach, R.H., and Gutmann, D.H. (2011). PET imaging for attention deficit preclinical drug testing in neurofibromatosis-1 mice. Exp. Neurol. *232*, 333–338.
36. Basu, T.N., Gutmann, D.H., Fletcher, J.A., Glover, T.W., Collins, F.S., and Downward, J. (1992). Aberrant regulation of ras proteins in malignant tumour cells from type 1 neurofibromatosis patients. Nature *356*, 713–715.
37. Bollag, G., Clapp, D.W., Shih, S., Adler, F., Zhang, Y.Y., Thompson, P., Lange, B.J., Freedman, M.H., McCormick, F., Jacks, T., and Shannon, K. (1996). Loss of NF1 results in activation of the Ras signaling pathway and leads to aberrant growth in haematopoietic cells. Nat. Genet. *12*, 144–148.
38. Froehlich, J.C., and Li, T.K. (1994). Opioid involvement in alcohol drinking. Ann. N Y Acad. Sci. *739*, 156–167.
39. Repunte-Canonigo, V., Herman, M.A., Kawamura, T., Kranzler, H.R., Sherva, R., Gelernter, J., Farrer, L.A., Roberto, M., and Sanna, P.P. (2015). Nf1 regulates alcohol dependence-associated excessive drinking and gamma-aminobutyric acid release in the central amygdala in mice and is associated with alcohol dependence in humans. Biol. Psychiatry *77*, 870–879.
40. Nogueiras, R., Romero-Picó, A., Vazquez, M.J., Novelle, M.G., López, M., and Diéguez, C. (2012). The opioid system and food intake: homeostatic and hedonic mechanisms. Obes. Facts *5*, 196–207.
41. Macey, T.A., Lowe, J.D., and Chavkin, C. (2006). Mu opioid receptor activation of ERK1/2 is GRK3 and arrestin dependent in striatal neurons. J. Biol. Chem. *281*, 34515–34524.
42. Urs, N.M., Daigle, T.L., and Caron, M.G. (2011). A dopamine D1 receptor-dependent β-arrestin signaling complex potentially regulates morphine-induced psychomotor activation but not reward in mice. Neuropsychopharmacology *36*, 551–558.
43. Kelly, E. (2013). Efficacy and ligand bias at the μ-opioid receptor. Br. J. Pharmacol. *169*, 1430–1446.
44. Violin, J.D., Crombie, A.L., Soergel, D.G., and Lark, M.W. (2014). Biased ligands at G-protein-coupled receptors: promise and progress. Trends Pharmacol. Sci. *35*, 308–316.
45. Banerjee, S., Crouse, N.R., Emnett, R.J., Gianino, S.M., and Gutmann, D.H. (2011). Neurofibromatosis-1 regulates mTOR-mediated astrocyte growth and glioma formation in a TSC/Rheb-independent manner. Proc. Natl. Acad. Sci. USA *108*, 15996–16001.
46. Turke, A.B., Song, Y., Costa, C., Cook, R., Arteaga, C.L., Asara, J.M., and Engelman, J.A. (2012). MEK inhibition leads to PI3K/AKT activation by relieving a negative feedback on ERBB receptors. Cancer Res. *72*, 3228–3237.
47. Ferner, R.E., and Gutmann, D.H. (2013). Neurofibromatosis type 1 (NF1): diagnosis and management. Handb. Clin. Neurol. *115*, 939–955.
48. Shilyansky, C., Lee, Y.S., and Silva, A.J. (2010). Molecular and cellular mechanisms of learning disabilities: a focus on NF1. Annu. Rev. Neurosci. *33*, 221–243.
49. Acosta, M.T., Kardel, P.G., Walsh, K.S., Rosenbaum, K.N., Gioia, G.A., and Packer, R.J. (2011). Lovastatin as treatment for neurocognitive deficits in neurofibromatosis type 1: phase I study. Pediatr. Neurol. *45*, 241–245.
50. van der Vaart, T., Plasschaert, E., Rietman, A.B., Renard, M., Oostenbrink, R., Vogels, A., de Wit, M.C., Descheemaeker, M.J., Vergouwe, Y., Catsman-Berrevoets, C.E., et al. (2013). Simvastatin for cognitive deficits and behavioural problems in patients with neurofibromatosis type 1 (NF1-SIMCODA): a randomised, placebo-controlled trial. Lancet Neurol. *12*, 1076–1083.

Current Biology, Volume *26*

Supplemental Information

NF1 Is a Direct G Protein Effector Essential for Opioid Signaling to Ras in the Striatum

Keqiang Xie, Lesley A. Colgan, Maria T. Dao, Brian S. Muntean, Laurie P. Sutton, Cesare Orlandi, Sanford L. Boye, Shannon E. Boye, Chien-Cheng Shih, Yuqing Li, Baoji Xu, Roy G. Smith, Ryohei Yasuda, and Kirill A. Martemyanov

Figure S1

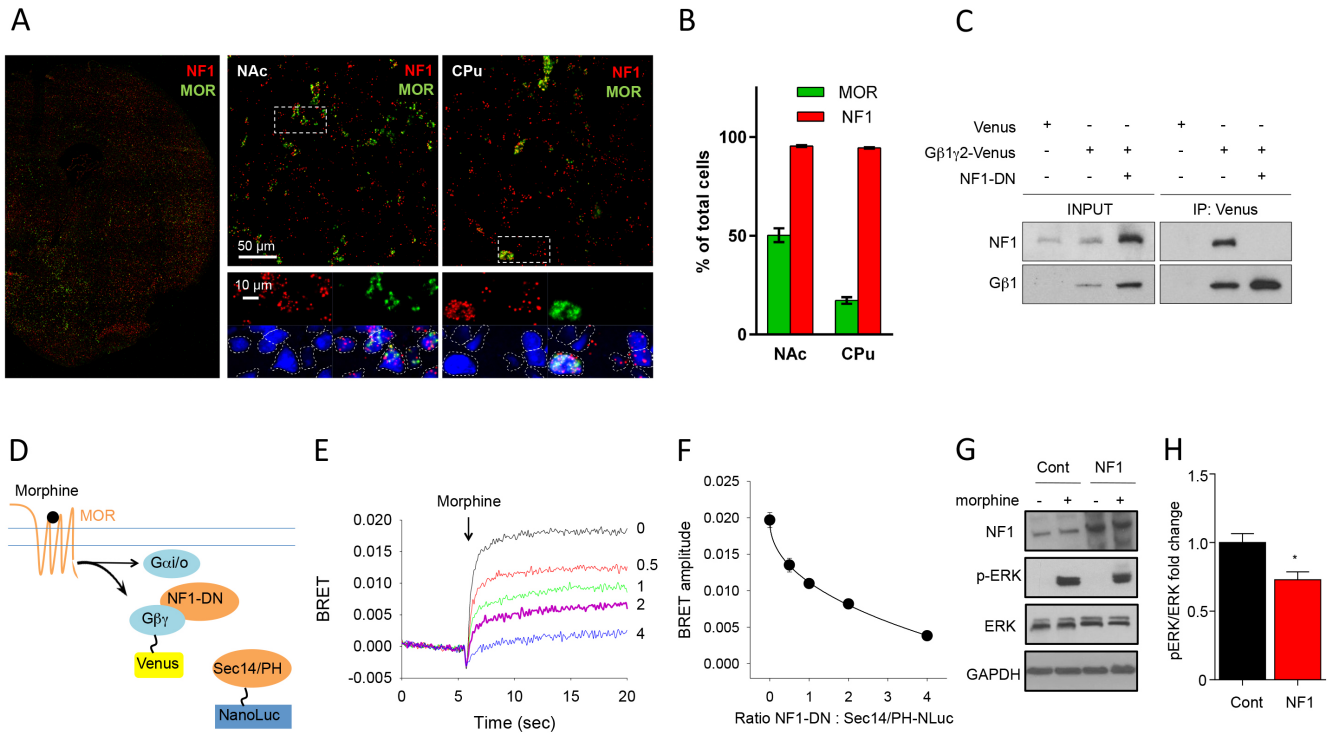
A
NF1
MOR
NAc
CPu
50 μm
10 μm
B
MOR
NF1
% of total cells
100
50
0
NAc
CPu
C
Venus
Gβ1γ2-Venus
NF1-DN
INPUT
IP: Venus
NF1
Gβ1
D
Morphine
MOR
Gαi/o
NF1-DN
Gβγ
Venus
Sec14/PH
NanoLuc
E
Morphine
BRET
Time (sec)
0
0.5
1
2
4
F
BRET amplitude
Ratio NF1-DN : Sec14/PH-NLuc
G
Cont
NF1
morphine
NF1
p-ERK
ERK
GAPDH
H
pERK/ERK fold change
Cont
NF1

Figure S2

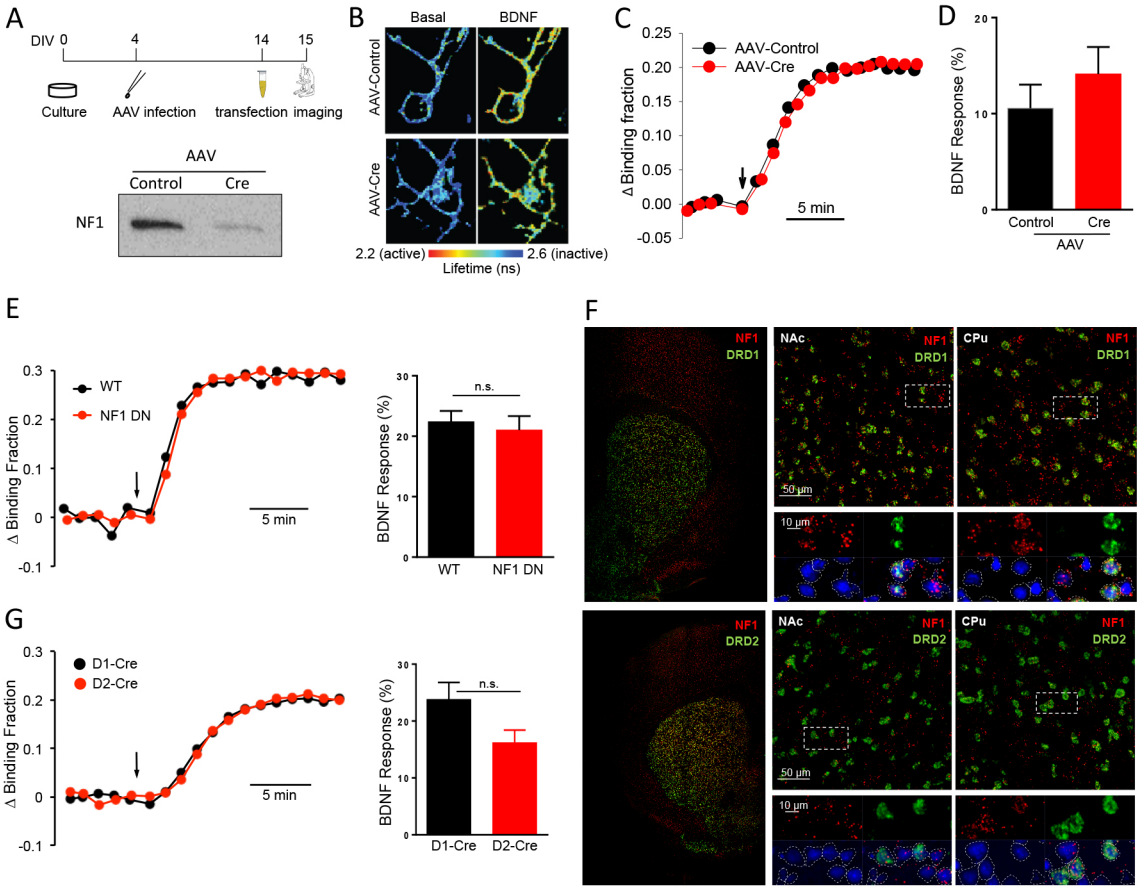
A
DIV 0
4
14
15
Culture
AAV infection
transfection
imaging
AAV
Control
Cre
NF1
B
Basal
BDNF
AAV-Control
AAV-Cre
2.2 (active)
2.6 (inactive)
Lifetime (ns)
C
AAV-Control
AAV-Cre
Δ Binding fraction
5 min
D
BDNF Response (%)
Control
Cre
AAV
E
WT
NF1 DN
Δ Binding Fraction
5 min
n.s.
BDNF Response (%)
WT
NF1 DN
F
NF1
DRD1
NAc
CPu
50 μm
10 μm
NF1
DRD2
G
D1-Cre
D2-Cre
Δ Binding Fraction
5 min
n.s.
BDNF Response (%)
D1-Cre
D2-Cre

Figure S3

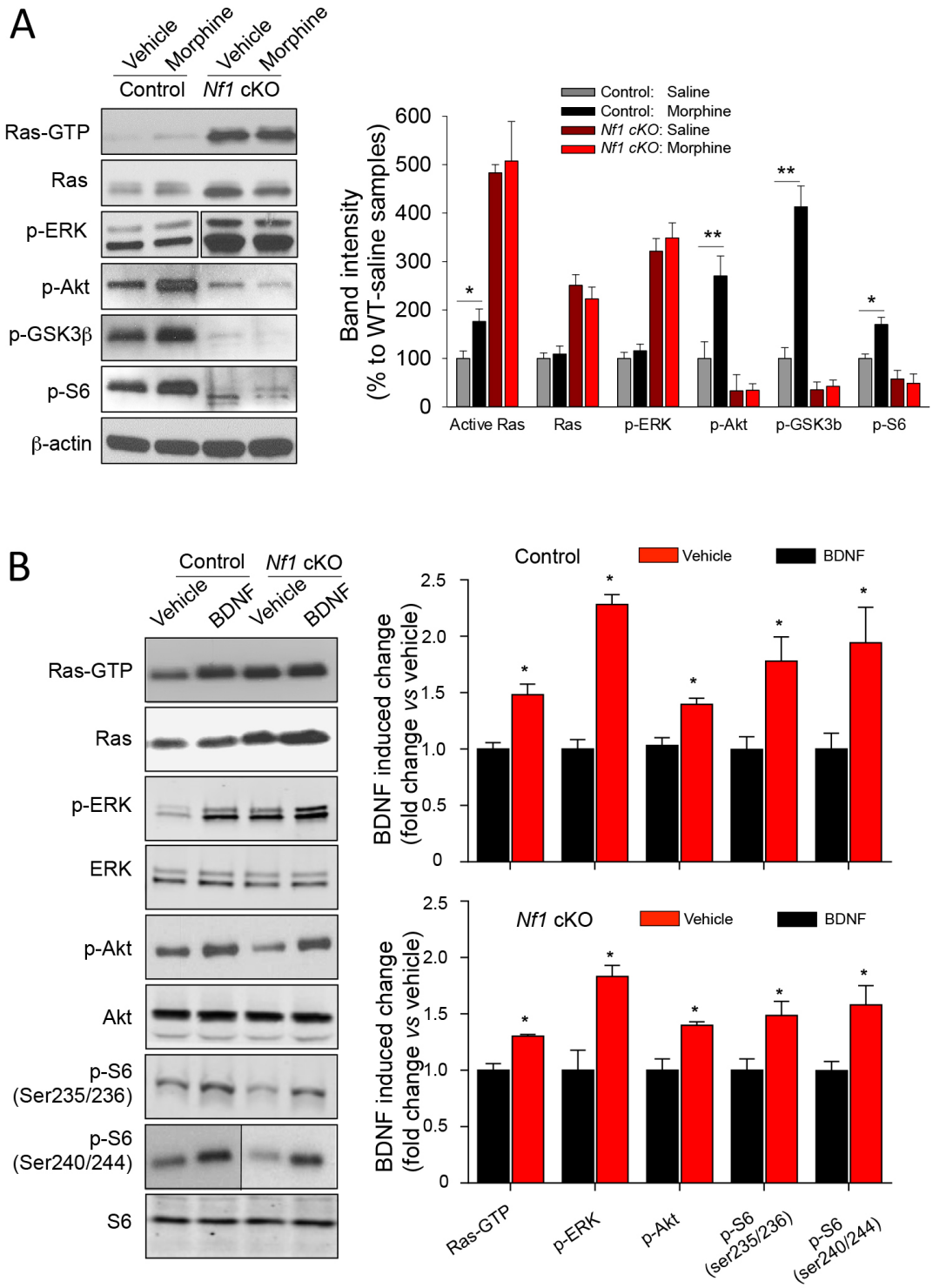
A
Vehicle
Morphine
Vehicle
Morphine
Control
Nf1 cKO
Ras-GTP
Ras
p-ERK
p-Akt
p-GSK3β
p-S6
β-actin
Control: Saline
Control: Morphine
Nf1 cKO: Saline
Nf1 cKO: Morphine
Band intensity (% to WT-saline samples)
600
500
400
300
200
100
0
*
**
**
*
Active Ras
Ras
p-ERK
p-Akt
p-GSK3b
p-S6
B
Control
Nf1 cKO
Vehicle
BDNF
Vehicle
BDNF
Ras-GTP
Ras
p-ERK
ERK
p-Akt
Akt
p-S6 (Ser235/236)
p-S6 (Ser240/244)
S6
Control
Vehicle
BDNF
BDNF induced change (fold change vs vehicle)
2.5
2.0
1.5
1.0
0.5
0
Nf1 cKO
Vehicle
BDNF
BDNF induced change (fold change vs vehicle)
Ras-GTP
p-ERK
p-Akt
p-S6 (ser235/236)
p-S6 (ser240/244)

Figure S4

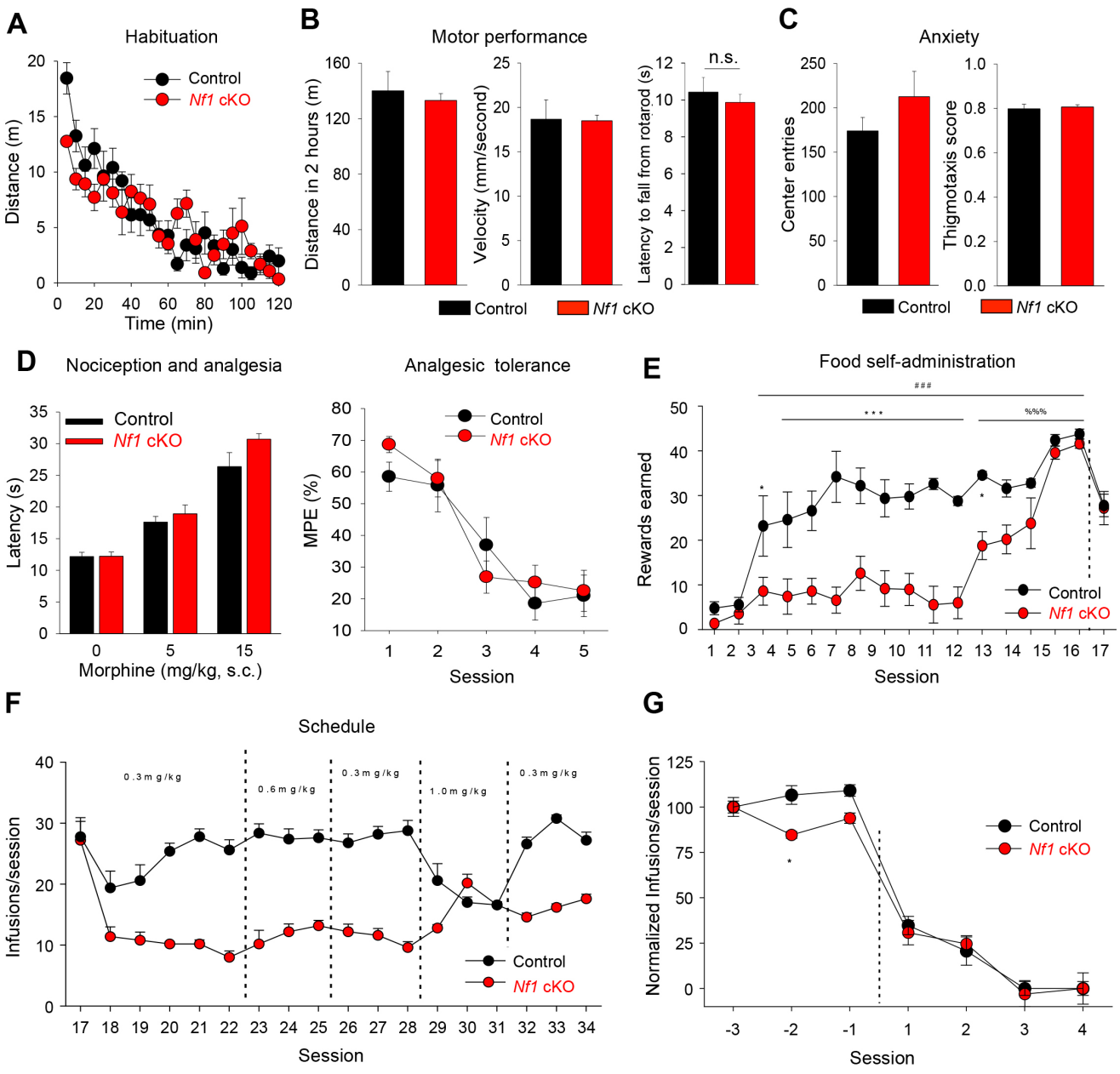
A
Habituation
Control
Nf1 cKO
Distance (m)
Time (min)
B
Motor performance
Distance in 2 hours (m)
Velocity (mm/second)
Latency to fall from rotarod (s)
n.s.
Control
Nf1 cKO
C
Anxiety
Center entries
Thigmotaxis score
Control
Nf1 cKO
D
Nociception and analgesia
Latency (s)
Morphine (mg/kg, s.c.)
Analgesic tolerance
MPE (%)
Session
E
Food self-administration
Rewards earned
Session
F
Schedule
0.3 mg/kg
0.6 mg/kg
1.0 mg/kg
Infusions/session
Session
G
Normalized Infusions/session
Session

SUPPLEMENTAL FIGURE LEGENDS

Figure S1, Related to Figure 1. Regulation of NF1 by MOR signaling. A, mRNAs for NF1 and MOR are extensively co-expressed in striatal neurons Representative image of a double in situ hybridization using probes against NF1 (red) and MOR (green) in the coronal section of dorsal (CPu) and ventral (NAc) striatum. Areas outlined by the box in the upper panels are shown enlarged in lower panels. Soma of neuron is defined by Nissl staining (blue) and its boundaries are delimited with a dashed line used to assign mRNA expression in individual neuron. **B**, Quantification of signal distribution across neuronal population. At least 4 images derived from 3 different coronal sections were counted using Nissl staining as a mask. Each image contained an average of 300 neurons. Error bars are SEM. **C**, Dominant negative NF1 construct (NF1-DN) prevents Gβγ binding to wild type NF1 endogenously present in the cells. HEK293T cells were transfected with either Venus-tagged Gβ1γ2 or Venus (control) with or without co-expression with NF1-DN. Following Gβγ immunoprecipitation by antibodies against Venus, proteins were detected by Western blotting using specific antibodies for Gβ1 and NF1. Representative experiment is shown. **D**, Schematics for the strategy for using NF1-DN construct to disrupt MOR-induced Gβγ interaction with Sec14/PH domains of NF1. Upon activation of MOR by morphine, Gβγ-Venus is released from Gαi/o subunits and becomes available to interact with NanoLuc tagged Sec14/PH domain of NF1 eliciting BRET response. The dominant negative construct NF1-DN comprises Sec14/PH domain and competes with NF1 binding preventing generation of the BRET signal. **E**, Representative BRET response traces produced by the application of morphine in the presence of various concentrations of NF1-DN construct delivered at the indicated ratios to Sec14/PH-NLuc construct. Note the inhibition of the signal generation as the ratio is increasing. **F**, Quantification of the dose-response relationship between an increase in NF1-DN concentration and maximal BRET amplitude. Error bars are SEM, n=3 experiments. **G**, Effect of NF1 overexpression in HEK293T cells on MOR-

mediated ERK phosphorylation. Cells were transfected with MOR and where indicated with full-length NF1 cDNA vector. Following treatment with 1 mM morphine for 5 min, cells were lysed and proteins were detected by Western blotting using indicated antibodies. **H**, Quantification of morphine-induced changes in pERK band between control cells and cells overexpressing NF1. Values were normalized to the control samples. *$p<0.05$, t-test, n=3 for each condition.

Figure S2, Related to Figure 3. NF1 does not affect Ras activation in cultured striatal neurons in response to BDNF application. **A**, Experimental outlines of Ras FLIM-FRET assay. *Insert*, Significant reduction of NF1 protein level after AAV-Cre infection. **B**, Representative fluorescence lifetime images before and after application of 10 ng/mL BDNF in cultures infected with either AAV-Cre virus or control AAV. **C**, Representative traces of changes in binding fraction in response to BDNF. **D**, Quantification of the peak change in binding fraction before and after BDNF stimulation. Data are represented as mean ± SEM. Unpaired t-test, $p= 0.3593$, n=7, 6. **E**, Representative traces of changes in binding fraction and quantification of the amplitude of responses to BDNF application in cultures transfected with NF1-DN construct as compared to control cultures transfected with an empty vector. Unpaired t-test $p=0.648$ n=8, 9. **F**, Fluorescent in situ hybridization examining expression of NF1 (red) in D1 receptor (D1R) and D2 receptor (D2R) containing striatal medium spiny neurons (green) in dorsal (CPu) and ventral (NAc) striatum. Neuronal cell bodies were stained with Nissl (blue), which is used as a mask when assigning signals to individual neurons. NF1 is found to be equally expressed by both D1R and D2R –containing neurons. We found 55±2% of NF1 positive MSNs in dorsal striatum and 45±2% in nucleus accumbens expressed D1R, while 37±2% of NF1 positive MSNs in both regions expressed D2R **G**, Representative traces of changes in binding fraction and quantification of the amplitude of responses to BDNF application in D1R-Cre and D2R-Cre cultures transfected with FLIM-FRET Flex Ras sensors. Unpaired t-test $p=0.06$ n=9, 8.

Figure S3, Related to Figure 4. NF1 inactivation in the striatum changes baseline levels of active Ras and downstream signaling pathway but does not abolish responses to BDNF. A, Representative Western blot data of active Ras and its downstream effector molecules (p-ERK, p-Akt) in striatal lysates when analyzed on the same side by side. Striata were dissected from 4 month-old *Nf1* cKO mice and Cre(-) control littermates and assayed for active Ras by pull down assay and Western blot analysis. Bar graphs show non-normalized quantification of Western blot data normalized to band densities in WT saline treated samples. Data are represented as mean ± SEM. **p<0.01, Student's t-test. **B**, Representative Western blot data of changes in active Ras and its downstream kinases in response to BDNF injection into the striatum. Four month-old *Nf1* cKO mice and Cre(-) control littermates were stereotaxically injected with BDNF or vehicle into the nucleus accumbens. Tissues removed 30 minutes later were analyzed for changes in activation of Ras and downstream signaling pathways by pull down assay and Western blotting. Bar graphs show quantification of band densities normalized to vehicle treated samples. Data are represented as mean ± SEM. **p<0.01, Student's t-test.

Figure S4, Related to Figure 5. Behavioral analysis of mice lacking NF1 in the striatum. **(A)** Evaluation of habituation to novel environment in the open field test. Naïve *Nf1* cKO mice and their control littermates were placed in the open field chamber and their activity was recorded for 2 hours. P>0.05, t-test, n=6-8 mice per group. **(B)** Quantification of typical mouse behavioral traits in the open field total related to motor performance: distance traveled and movement velocity as well as evaluation of motor coordination in the rotarod task. **(C)** Anxiety traits evaluated in the open field: center entries and thigmotaxis score. **(D)** *Nf1* cKO mice show comparable basal nociceptive thresholds, analgesic sensitivity and tolerance to morphine. In tolerance assays, mice were monitored by the hot plate test 30 min following morphine treatment (15 mg/kg) for 5 days. Two-Way ANOVA post hoc Tukey's test p=0.38 (n=4-5 mice per each group). **(E)** Operant conditioning of mice in self-administration task during food training paradigm. Cohort comparison for food self-administration over 1 hour session courses and

ability to learn lever pressing for food reward to meet criteria (dashed line). Genotype vs. Session (n=5 per group), interaction $p<0.001$, Genotype $p=0.0017$, Session $p<0.001$. Data is expressed as mean ± SEM *$p<0.05$, ***$p<0.001$ genotype comparison, $^{###}p<0.001$ WT compared to Day 1 WT, $^{\%\%\%}p<0.001$ KO compared to Day 1 KO, two-way ANOVA with Bonferroni test. Vertical dashed line marks switching mice from food to morphine. **(F)** Complete profile of mouse performance in self-administration task. Mice were allowed access to varying concentrations of drugs in consecutive sessions and their lever pressing behavior was monitored. (**G**) Extinction of lever pressing behavior upon substitution of morphine (0.3 mg/kg) with saline. No genotype differences were noted. Vertical dashed line marks switching mice from morphine to saline.

SUPPLEMENTAL EXPERIMENTAL PROCEDURES

Mice and DNA constructs

Generation of *Nf1*$^{flx/flx}$ [S1] and *Rgs9-Cre* [S2] mice was described previously. To assess the role of NF1 in striatal neurons, we crossed *Nf1*$^{flx/flx}$ mice with *Rgs9-Cre* driver line to generate striatal specific NF1 conditional knockout (*Nf1* cKO) mice. *Nf1*$^{flx/flx}$ Cre(-) control littermates (2–4 months old) derived from heterozygous breeding pairs were used for all experiments. D1-Cre (Drd1-Cre; EY262; stock# 017264-UCD) and D2-Cre (Drd2-Cre; ER44; MMRRC Stock #: 017263-UCD) were obtained from MMRRC. All mice are on the C57/Bl6 background. Mice were housed in groups on a 12 h light–dark cycle with food and water available *ad libitum*. All procedures were approved by the Institutional Animal Care and Use Committee (IACUC) at The Scripps Research Institute.

Sec14 (1566 – 1735 a.a.), PH (1736 – 1837 a.a.), Sec14/PH (1566 – 1837 a.a.) and GRD/Sec14/PH (1198 – 1837 a.a.) were amplified from full length of NF1 template (gift from Dr. Frank McCormick in UCSF). Sec14/PH (1566 – 1837 a.a.) fused with N-terminal membrane-targeting sequence of Lyn kinase (GCIKSKRKDKD) cloned into pcDNA3.1 was used as NF1-dominant negative (NF1-DN).

NanoLuc™ luciferase (Nlc) was amplified from pNL1.1.CMV vector (Promega). Fusion constructs (Sec14-Nlc, PH-Nlc, Sec14/PH-Nlc, NF1-Nlc) were made by In-Fusion® HD Cloning Kit (Clontech) with membrane-targeting sequence of Lyn kinase (GCIKSKRKDKD) in the N terminal of fusion proteins except NF1-Nlc. Sec14/PH and GRD/Sec14/PH were subcloned in pGEX-2T E. Coli expression vector. BRET reporter constructs Venus155-239-Gβ1, Venus1-155-Gγ2, Venus-H-Ras and masGRK3ct were gifts from Dr. Nevin A. Lambert (Medical College of Georgia), and HA tagged μ-opioid receptor (HA-MOR) was a gift from Dr. Ping-Yee Law (University of Minnesota). Rat cDNA mammalian expression clones for Gαo in pCMV5 were gifts from Dr. Hiroshi Itoh (Nara Institute of Science and Technology). Catalytic domain of sos1 (564 – 1049 a.a.) and full length of N-Ras were subcloned in pET28b *E. Coli* expression vector. FLIM-FRET ras sensor GFP-HRas and RFP-Raf

binding domain-RFP were constructed as previously described [S3]. Reverse orientation of Ras FRET donor (HRas-mGFP) flanked with the flip-excision (FLEX) switch sequences was cloned into a pcDNA3.1 to generate conditional FRET donor construct whose expression is dependent on Cre recombinase.

Primary cultures of striatal neurons

Primary cultures of striatal neurons were prepared as described previously with minor modifications [S4]. Briefly, striata were extracted from neonatal pups from wild type C57Bl6, *Nf1*$^{flx/flx}$, D1-Cre or D2-Cre mice and placed into an ice-cold HBSS/FBS solution: Hank's Balanced Salt Solution (Sigma; St. Louis, MO), 4.2 mM NaHCO3, 1 mM HEPES, and 20 % FBS. Tissue was washed twice with HBSS/FBS, and then 3 times with HBSS alone. Striatum tissues were digested at room temperature for 15 min with 0.3 mg/mL Papain (Worthington) in a solution containing137 mM NaCl, 5 mM KCl, 7 mM Na2HPO4, and 25 mM HEPES (pH 7.2). Tissue was washed twice with HBSS/FBS and 3 times with HBSS alone, and then mechanically-dissociated in HBSS (supplemented with 12 mM MgSO4) using Pasteur pipettes of decreasing diameter. Neurons were pelleted by centrifugation (600 g for 10 min at 4 °C) and plated onto 12-mm glass coverslips pre-coated with Matrigel (BD Biosciences; San Jose, CA). Neurons were allowed to adhere for 1-2 hours prior to adding pre-warmed culture medium consisting of Neurobasal A (Life Technologies; Carlsbad, CA), 2 mM GlutaMAX-I (Life Technologies, Carlsbad, CA), 2 % B-27 supplement. Neurons were incubated at 37°C/5% CO2, and half of medium was replaced with fresh medium every 3 days. Neurons were infected with AAV-Cre or AAV-GFP control virus on DIV4 (1:20,000 dilution). Ras FRET sensors with/without NF1-DN construct in pcDNA3.1 were transfected on DIV 14 using lipofectamine 2000 (Invitrogen). For conditional FRET sensor experiments, Flexed FRETdonor (Flex-HRas-mGFP) was co-transfected with FRET acceptor (Raf-RBD-mRFP) in striatal neuron cultures derived from *D1*-Cre or *D2*-Cre neonatal mice.

Protein sample preparation, immunoprecipitation and Western blot

Striatal tissue (~15 mg) or transfected HEK293T cells were homogenized by sonication in lysis buffer (1×PBS, 150 mM NaCl, 0.5 % n-dodecanoylsucrose containing complete protease inhibitor cocktail (Roche) and phosphatase inhibitor cocktail 1 and 2 (Sigma). Homogenate was centrifuged at 16,000 g for 15 min. Supernatant was incubated with 3 μg antibodies as indicated and 10 μL of protein G beads for 1 hours at 4 °C. Beads were washed 3 times with lysis buffer. Protein sample was eluted in SDS sample buffer, boiled for 5 min, and resolved on SDS-PAGE gel, transferred onto PVDF membrane and subjected to Western blot analyses. The following specific antibodies were used for either immonoprecipitation or Western blot: c-myc (Genescript), Gβ1 (gift from Dr. Barry M. Willardson, Brigham Young University), NF1 (Bethyl Laboratories), GFP (Roche), p-ERK1/2, ERK, p-Akt (S473), Akt, p-S6 (235/236 and 240/244), S6, p-GSK3β, GSK3β (Cell Signaling Technology).

Recombinant proteins and membrane preparations

Recombinant complexes of Gβ1 with His-tagged Gγ2 were expressed in Sf9/baculovirus system and purified as described [S5]. GST-tagged Sec14/PH as well as GRD/Sec14/PH were expressed in BL21 (DE3) *E. coli* strain and purified by affinity chromatography on glutathione-Sepharose 4B beads (GE healthcare) as described previously [S5]. His-tagged catalytic domain of sos1 and N-Ras were expressed in BL21 (DE3) E. Coli strain and purified by affinity chromatography on HisTALON columns using AKTA Fast Protein Liquid Chromatography (FPLC) system. The purity of recombinant proteins was assessed by Coomasie staining following gel separation and was found to be at least 80 %.

Pull down assay

GST pull down assay was performed as described previously with minor modifications [S4]. Briefly, purified recombinant GST-Sec14/PH fusion proteins or GST control protein (0.25 μM) and purified Gβ1γ2 proteins (0.25 μM) were co-incubated with 20 μl of 50% glutathione agarose beads slurry (GE

Healthcare) in binding buffer (20 mM Tris, pH 7.2, 300 mM NaCl, 100 μM polyoxyethylene 10 Lauryl ether, 50 μg/ml bovine serum albumin) for 1 hour at 4 °C. The beads were washed with binding buffer 3 times. Proteins retained by the beads were eluted in SDS sample buffer and detected by anti-Gβ1 antibody by immunoblotting. Membrane blot were stained with Ponceau S to visualize the GST fusion protein or GST control protein.

Bioluminescence resonance energy transfer (BRET)

A new version of bioluminescence resonance energy transfer (BRET) assay NanoBRET consisting of NanoLuc luciferase technology was performed to visualize the interaction between Nanoluc (Nlc)-tagged energy donor and Venus-tagged energy acceptor.

For membrane recruitment assay, Venus was targeted to plasma membrane through fusion to 25 amino acid C-terminal fragments of HRas [S6] and BRET assay was used to monitor interaction between NF1-Nlc and membrane attached venus. HEK293T cells were transfected with μ-opioid receptor, Gαo, Gβ1, Gγ2, NF1-Nlc, Venus-HRas, with or without masGRK3ct constructs. 24 hours later, after the Nano-Glo Luciferase substrate was added, BRET measurements were made using a micro plate reader (POLARstar Omega; BMG Labtech) equipped with two emission photomultiplier tubes, allowing the detection of two emissions simultaneously with resolution of 50 milliseconds for every data point. All measurements were performed at room temperature. The raw BRET signal is determined by calculating the ration of the light emitted by the venus (535 nm) over the light emitted by the nanoluc (475 nm). The average baseline value recorded before stimulation was subtracted from raw BRET signal values, and the resulting BRET was plotted over the time. Gβ1γ2 scavenger (GRK3ct) was co-transfected to block Gβγ effects.

To determine the specific interaction between Sec14/PH and Gβ1γ2, different ratio of acceptor (Gβ1γ2-Venus) vs donor (Sec14-Nlc, PH-Nlc or Sec14/PH-Nlc) cDNA amount were transiently transfected to

HEK293T cells. The pNL1.1.CMV (Nlc) was included as a negative control. Cells were then used for NanoBRET measurement 24 hours later. The average baseline value recorded from samples without acceptor expression was subtracted from raw BRET signal values, and the resulting BRET was plotted over the ratio of acceptor/donor. Signal curve was fitted with hyperbola nonlinear regression to obtain maximal BRET ratios. NanoLuc luciferase alone was used as a control.

NanoBRET was also applied to measure the dynamic interaction of Sec14/PH-Nlc and Gβ1γ2-Venus in response to the action of G protein signaling in living cells as previously described with slight modifications [S5]. Briefly, HEK293T cells were transfected with μ-opioid receptor, Gαo, Venus155-239-Gβ1, Venus1-155-Gγ2, Sec14/PH-Nlc, with or without masGRK3ct constructs at a 1:2:1:1:1:1 ratio. Cells were then used for NanoBRET measurement 24 hours later. The average baseline value recorded before agonist application was subtracted from raw BRET signal values, and the resulting BRET was plotted over the time. Dose response of BRET amplitudes were fitted with hyperbola nonlinear regression to obtain EC50 of morphine. Co-transfection with Gβ1γ2 scavenger (GRK3ct) was used to block Gβ1γ2 effects. . Co-transfection with Sec14/PH and increasing amounts of Sec14/PH-Nlc was used to demonstrate the competition of NF1 binding to Gβγ.

GTPase activity assays

Single-turnover GTPase assays using recombinant proteins were conducted as described previously [S7]. Pre-loaded [γ-^{32}P]-GTP-Ras undergoes single turnover GTP hydrolysis resulting in inorganic phosphatase ($^{32}P_i$) and GDP-Ras. RasGAP protein NF1 accelerates GTP hydrolysis. Purified N-Ras (2 μM) was pre-loaded with 4 μM [γ-^{32}P]-GTP (25 Ci/mmol, MP Biomedicals) in charging buffer (20 mM Tris-HCl pH 7.8, 100 mM NaCl, 1 mM DTT, 4 mM EDTA) for 5 min at 37 °C. The mixture is placed on ice and MgCl2 was added to a final concentration of 17 mM. The buffer of [γ-^{32}P]-GTP-bound N-Ras was exchanged to GTPase buffer (20 mM Tris-HCl pH7.8, 100 mM NaCl, 5 mM MgCl2, 100 μM

polyoxyethylene 10 lauryl ether, 1 mM DTT) using protein desalting spin column (Pierce). 6.67 μL of the [γ-^{32}P]-GTP-Ras solution is removed (time zero) directly to 100 μL of quench solution (6 % perchloric acid). GTPase assays were performed at 37 °C in GTPase buffer. Final concentrations in the reactions were 0.3 μM N-Ras, 0.5 μM Gβ1γ2, 65 nM GRD/Sec14/PH. Samples (20 μL) were removed at 2-, 5-, 10-, 20-, and 30-min intervals to 100 μL of 6 % perchloric acid. ^{32}Pi (Pi, inorganic phosphate) released from hydrolyzed GTP was determined by activated charcoal assay [S8]. The amount of radioactivity was determined by scintillation counting. Complete (100 %) GTP hydrolysis was performed in the presence of excess GRD/Sec14/PH (1.5 μM) for at least 1 hour. Percentage of GTP hydrolysis was calculated as (time point − time zero)/(100 % GTP hydrolysis − time zero) × 100 %. To determine values for speed of GTP hydrolysis (1/τ), the data were fitted to exponential equation using non-linear regression.

For multiple turnover GTPase assays, GTP/GDP exchange of Ras is catalyzed by RasGEF protein sos1. [γ-^{32}P]-GTP-Ras undergoes NF1-catalzyed GTP hydrolysis resulting in $^{32}P_i$ and GDP-Ras. Ras exhibits multiple turnover of GTP/GDP exchange and GTP hydrolysis. The purified proteins (0.5 μM N-Ras, 5 μM sos1, 25 nM GRD/Sec14/PH, and (0, 0.1, 0.3 or 1μM Gβγ) were incubated with 50 μM [γ-^{32}P]-GTP in GTPase buffer at 37 °C for 20 min (a period in which the velocity of P_i liberation was constant) in the total volume of 20 μL. Reactions were stopped by adding 100 μL quench solution. Inorganic phosphate released from hydrolyzed GTP was determined by activated charcoal assay. Complete (100 %) GTP hydrolysis was performed in the presence of excess GRD/Sec14/PH (1.5 μM), and was used to calculate percentage of GTP hydrolysis. Data were fitted with hyperbolic decay equation to get IC50 of Gβγ. Control reactions were performed to ensure that multiple turnover conditions are maintained and that GDP/GTP exchange is not limiting the GTP hydrolysis.

Two-photon fluorescence microscopy and two-photon fluorescence lifetime imaging

mEGFP was tagged to the N terminus of HRas, and mRFP was attached to both termini of Ras binding domain of Raf1 (RBD), which binds selectively to active Ras. FRET between mEGFP and mRFP increases when HRas is activated. Fluorescence lifetime measurements of mEGFP were used as a quantitative readout of FRET. Imaging was done using a custom-built two-photon microscope equipped with a fluorescence lifetime imaging system. Fluorescence was excited using a two-photon excitation at 920 nm by a Coherent chameleon pulsed laser. Laser intensity was controlled with electro-optical modulators (350–80 LA; Conoptics) before being scanned by galvano-scanning mirrors focused into the sample by an objective (60×, 0.9 numerical aperture; Olympus). Emitted fluorescence was divided with a dichroic mirror (565 nm; Chroma) and detected with cooled photomultiplier tubes (H7422–40 for green and R3896 for red; Hamamatsu) after wavelength filters (HQ510/70–2p for green and HQ620/90–2p for red; Chroma Technology). Fluorescence intensity images were acquired by ScanImage using a data acquisition board (PCI-6110; National Instruments) and fluorescence lifetime images were acquired with a time-correlated single photon counting system (SPC-150; Becker and Hickl). Binding fraction was calculated as described previously [S3].

On day in vitro (DIV) 0, striatal neurons were cultured from neonatal *Nf1*$^{flx/flx}$ pups. Neurons were infected with AAV virus on DIV4. Ras FRET sensors were transfected on DIV 14. FLIM-FRET assay were performed 1 day after transfection. Striatal neuron cultures from neonatal NF1flx/flx mice infected with either control or Cre-RFP viruses were washed and imaged in HEPES buffered aCSF containing 1uM Tetrototoxin (TTX) to inhibit spontaneous activity. After obtaining baseline images, morphine (10 μM, Sigma) or BDNF (10 ng/mL, R&D Systems) were bath applied and fluorescence lifetime was monitored. *D1-Cre* and *D2-Cre* striatal neurons were cultured on DIV0 and co-transfected with Lipofectamine 2000 on DIV 14-15 with Flex-mEGFP-HRas and mRFP-RBD-mRFP at a 1:1 ratio using 0.25 μg of each construct per 12 mm coverslip. Two-photon microcopy was used 24-30 hours post transfection to image fluorescence lifetime and measure FRET between Ras sensors.

Acute morphine or BDNF treatment and active Ras pull down assay

Mice were injected subcutaneously with morphine (20 mg/kg) or saline (10 ml/kg) and sacrificed 1 hours post-injection. BDNF (0.75 μg/side) or its vehicle was bilaterally infused into the NAc (see Stereotaxic surgery section) and sacrificed 30min post-injection. The striatum was immediately dissected and subjected to active Ras assay using active Ras pull down and detection kit (Thermo Scientific) following manufacturer's instructions.

Adeno-associated virus generation and delivery

Reverse orientation dominant negative NF1 (NF1-DN, Sec14/PH (1566 – 1837 a.a.) fused with N-terminal membrane-targeting sequence of Lyn kinase (GCIKSKRKDKD) and C-terminal P2A sequence (GSGATNFSLLKQAGDVEENPGP) and GFP was cloned into vector plasmid containing a truncated version of the ubiquitous CBA promoter, which is a fusion of the chicken beta actin promoter and the CMV immediate-early cytomegalovirus enhancer (smCBA), the flip-excision (FLEX) switch sequence, a woodchuck hepatitis virus posttranscriptional regulatory element (WPRE) sequence, SV40 polyA sequence, and two AAV2-based inverted terminal repeats required for recombinant adeno-associated virus (AAV) production. AAV8(Y733F)-smCBA-FLEX-NF1-DN-P2A-GFP vector was packaged and purified according to previously published methods [S9, S10].

Stereotaxic surgery

Mice were anesthetized with 1-2% isoflurane in oxygen on stereotaxic frame (KOPF 900, CA USA). AVV8-smCBA-FLEX-NFL-DN-P2A-GFP (Biovector Labs, Malvern PA USA) or BDNF (0.75 μg/side; R&D Systems, Minneapolis, MN USA) was bilaterally microinjected into NAc using gastight microsyringes (Hamilton 1800 series, Reno NV USA), Tygon tubing (Palmer Cole, Vernon Hills IL USA), 28-gauge piston needles and pump (World Precision Instruments, Sarasota FL USA). Stereotaxic coordinates for NAc were as followed: AP +1.1mm, ±1.0mm ML, and -3.8mm DV. Mice were injected

at the rate of 0.3µl over 5 minutes per side and were kept in place for an additional 5 minutes to ensure adequate diffusion. Mice were given two weeks of recovery for AAV expression.

Behavioral assays

Locomotion was evaluated in automated video tracking ANY-maze open field chambers (Stoelting) under illuminated conditions. Mice were habituated to testing room for 1 hour before the test on each day. One the first day, mice were placed in the chambers without injection, and allowed to explore the novel chamber for 2 hours. On the test day, mice were then injected with saline (10 mL/kg, s.c.) or morphine (2, 5, 10 or 20 mg/kg) and then immediately placed in the open-field chambers. Activity was then monitored for 3 hrs. Dose dependence morphine treatments were done on the same mice starting from low dose first with 2-day interval between different doses. Horizontal activity was measured in terms of the total distance traveled in the monitoring period or distance traveled in 5-min intervals. Thigmotaxis (wall hugging) for each subject was determined by dividing the distance traveled in the 10-cm-wide perimeter of the chamber by the total distance traveled during the 2-hour session.

Accelerating rotarod performance was tested using a five-station rotarod treadmill (IITC Rotarod, IITC Life Science). Mice of either gender from 8 to 9 week-old were used in this test. After placing a mouse on the rod, the rod was accelerated from 8 to 22 rpm in 2 min. The endurance (s) of mice on the rotarod and the terminal speed (rpm) was measured by time to fall to the floor of the apparatus or to turn one full revolution while hanging onto the drum.

The hot plate paw-lick test was performed on a platform heated to 54 °C with a cutoff of 40 second. Latency to paw lick or jump was recorded. Baseline responses were determined for each mouse before drug injection. Mice were injected with a volume of 100 µL per 10 g of body weight of morphine sulfate (s.c., 10 mg/kg), 30 min after acquiring baseline response. The analgesia response was tested 45 min after injection. The antinociceptive response was calculated as a percentage of maximal possible effect (MPE), where $\text{MPE } \% = (\text{final} - \text{baseline})/(40 - \text{baseline}) \times 100\ \%$.

Conditioned place preference (CPP) was conducted using a two-chamber box with a tunnel adjoining the chambers in which each chamber was distinguished by different color and floor texture (Stoelting Co, Wood Dale, IL). The CPP procedure consisted of four phases: habituation, preconditioning, conditioning and post-conditioning test. Time spent in each chamber was recorded by automated video tracking ANY-maze software (Stoelting). On the first day, each mouse was free to explore the two compartments for a 20-min period (habituation). On the second day, the time each mouse spent in each compartment was recorded for a 30-min period (pre-conditioning). On the third day, mice received morphine (5 or 15 mg/kg, s.c.) and immediately confined for 30 minutes in one compartment. On the fourth day, animals received a saline injection and paired with the other compartment for 30 minutes. There was a total of three drug sessions and three saline sessions (conditioning). On the test day, day nine, mice were allowed free access to all compartments for 30min (post-conditioning). Place preference (s) was assessed by calculating the difference between time spent in drug-paired compartment and time spent in saline-paired compartment.

Self-administration

Prior to drug self-administration, mice were subjected to food training paradigm in operant conditioning chambers (14 x 12.7 x 16cm; Med Associates, St. Albans VT USA) housed inside standard sound attenuating cubicles (56 x 38 x 40.6cm). Mice were fasted overnight to provide learning incentive and maintained to 85% of pre-fasted body weight. Operant chambers were equipped with two retractable levers, two light sources paired with levers, and dispenser for food pellets. Mice were trained to differentiate between two levers, one lever paired with food reward and other with no consequences. Each mouse was trained at FR1TO20 until enough food rewards were obtained before gradually

increasing to FR5TO20. Once all mice obtained at least 20 food rewards within an hour session for 3 consecutive days, they underwent surgery for jugular catheter implantation.

Catheters were made in house which consisted of 6 cm length silastic tubing fitted into guided cannula (Plastics One, Wallingford, CT). Cannulas were bent to curved right angle and encased in dental acrylic. Mice were placed on ad lib food 48 hours prior to surgery. Mice were anesthetized with 1-3% isoflurane in oxygen and implanted with indwelling intravenous catheters threaded into right external jugular vein from animals' back where guide cannula was situated.

Mice were allowed one-week post-surgery recovery and placed into operant chamber to ensure food training memory was stabilized. Food was replaced with morphine infusions (0.3mg/kg/infusion) for 6 consecutive days under identical conditions. Once all mice had learned to self-administer morphine, which is defined had by minimum of 15 infusions/session for three consecutive days with minimum response ratio of 5:1 between active and inactive levers and less than 20% variation of running mean without any increase or decrease trend, they were placed onto dose response schedule of 0.6mg/kg, 1.0 mg/kg and saline. Each dose was repeated for three consecutive days, they were switched to baseline (0.3mg/kg/infusion) for an additional three days to ensure that response was similar. Before and after each session, catheters were flush with 0.1ml of 10% heparin in saline. Catheters were tested for patency after each session by drawing back syringe for presence of blood during catheter flush.

Histology

Mice were anesthetized with Avertin (tribromoethanol) and perfused transcardially with phosphate buffered saline (PBS) and 4% paraformaldehyde (PFA). Brains were collected and postfixed in 4% PFA overnight, and stored in 30% sucrose solution for cryoprotection for 3 days. Brain sectioning was performed with 50 μm interval by sliding microtome (SM2000R, Leica). We stored sample slices in PBS at 4ºC or at -20ºC in antifreeze solution for long-term storage. Stereo Investigator software

(MicroBrightField Inc.) was used to measure the volume of striatum [S11]. The analysis was performed blinded to the genotypes.

In Situ Hybridization

The mRNA expression of NF1, MOR, DRD1 and DRD2 in the striatum was evaluated with ViewRNA^{TM} 2-plex *In Situ* Hybridization Assay (Panomics; Santa Clara, USA) using the following probe sets: NF1 (NM_010897; Cat# VB1-13578), MOR (NM_001039652; Cat# VB6-17469), DRD1 (NM_010076; Cat# VB6-12478) and DRD2 (NM_010077; Cat# VB6-16550). The procedure was previously described [S12]. Briefly, mouse brains were embedded in OCT, flash frozen in liquid nitrogen, cut in 14 μm coronal sections and rapidly fixed in 4% paraformaldehyde for 10'. Sections were then washed and incubated for 2h/RT in pre-hybridization mix (50% deionized formamide, 5X SSC, 5X Denhardt's solution, 250 μg/ml yeast tRNA, 500μg/ml sonicated salmon sperm DNA), followed by overnight incubation at 40ºC with Panomics hybridization solution containing TYPE 1 and TYPE 6 QuantiGene ViewRNA probe sets (DRD1 and DRD2 diluted 1:200; NF1 and MOR 1:50). Sections were then processed according to manufacturer's instructions. To identify the soma of the cells, each section was counterstained with NeuroTrace 435/455 Blue Fluorescent Nissl Stain (Molecular Probes, 1:100) and mounted using Fluoromont-G (SouthernBiotech). All the images were generated at The Light Microscopy Facility, Max Planck Florida Institute, using a LSM 780 Zeiss confocal microscope. Image acquisition and processing were accomplished using ZEN 2011 software (Carl Zeiss) with only minor manipulations of the images setting the fluorescence intensity in non-saturating conditions and maintaining similar parameters for each acquired image. The number of neurons positive for the expression of each gene was counted using FIJI software. At least four images for Nucleus Accumbens and four for Caudate-Putamen were counted and averaged. Approximately 300 neurons were present in each image.

SUPPLEMENTAL REFERENCES

S1. Zhu, Y., Romero, M.I., Ghosh, P., Ye, Z., Charnay, P., Rushing, E.J., Marth, J.D., and Parada, L.F. (2001). Ablation of NF1 function in neurons induces abnormal development of cerebral cortex and reactive gliosis in the brain. Genes Dev *15*, 859-876.

S2. Dang, M.T., Yokoi, F., Yin, H.H., Lovinger, D.M., Wang, Y., and Li, Y. (2006). Disrupted motor learning and long-term synaptic plasticity in mice lacking NMDAR1 in the striatum. Proc Natl Acad Sci U S A *103*, 15254-15259.

S3. Oliveira, A.F., and Yasuda, R. (2013). An improved Ras sensor for highly sensitive and quantitative FRET-FLIM imaging. PLoS One *8*, e52874.

S4. Xie, K., Allen, K.L., Kourrich, S., Colon-Saez, J., Thomas, M.J., Wickman, K., and Martemyanov, K.A. (2010). Gbeta5 recruits R7 RGS proteins to GIRK channels to regulate the timing of neuronal inhibitory signaling. Nat Neurosci *13*, 661-663.

S5. Xie, K., Masuho, I., Brand, C., Dessauer, C.W., and Martemyanov, K.A. (2012). The complex of G protein regulator RGS9-2 and Gbeta(5) controls sensitization and signaling kinetics of type 5 adenylyl cyclase in the striatum. Sci Signal *5*, ra63.

S6. Lan, T.H., Liu, Q., Li, C., Wu, G., and Lambert, N.A. (2012). Sensitive and high resolution localization and tracking of membrane proteins in live cells with BRET. Traffic *13*, 1450-1456.

S7. Self, A.J., and Hall, A. (1995). Measurement of intrinsic nucleotide exchange and GTP hydrolysis rates. Methods Enzymol *256*, 67-76.

S8. Cowan, C.W., Wensel, T.G., and Arshavsky, V.Y. (2000). Enzymology of GTPase acceleration in phototransduction. Methods Enzymol *315*, 524-538.

S9. Jacobson, S.G., Acland, G.M., Aguirre, G.D., Aleman, T.S., Schwartz, S.B., Cideciyan, A.V., Zeiss, C.J., Komaromy, A.M., Kaushal, S., Roman, A.J., et al. (2006). Safety of recombinant adeno-associated virus type 2-RPE65 vector delivered by ocular subretinal injection. Mol Ther *13*, 1074-1084.

S10. Zolotukhin, S., Potter, M., Zolotukhin, I., Sakai, Y., Loiler, S., Fraites, T.J., Jr., Chiodo, V.A., Phillipsberg, T., Muzyczka, N., Hauswirth, W.W., et al. (2002). Production and purification of serotype 1, 2, and 5 recombinant adeno-associated viral vectors. Methods *28*, 158-167.

S11. Baydyuk, M., Russell, T., Liao, G.Y., Zang, K., An, J.J., Reichardt, L.F., and Xu, B. (2011). TrkB receptor controls striatal formation by regulating the number of newborn striatal neurons. Proc Natl Acad Sci U S A *108*, 1669-1674.

S12. Sutton, L.P., Ostrovskaya, O., Dao, M., Xie, K., Orlandi, C., Smith, R., Wee, S., and Martemyanov, K.A. (2015). Regulator of G-Protein Signaling 7 Regulates Reward Behavior by Controlling Opioid Signaling in the Striatum. Biol Psychiatry.